



1 **In situ measurements of desert dust particles above the western**
2 **Mediterranean Sea with the balloon-borne Light Optical Aerosol**
3 **Counter/sizer (LOAC) during the ChArMEx campaign of summer 2013**

4
5 Jean-Baptiste Renard¹, François Dulac², Pierre Durand³, Quentin Bourgeois⁴, Cyrielle Denjean⁵,
6 Damien Vignelles¹, Benoit Couté¹, Matthieu Jeannot^{1,a}, Nicolas Verdier⁶, Marc Mallet^{3,b}

7
8 ¹Laboratoire de Physique et Chimie de l'Environnement et de l'Espace (LPC2E), UMR CNRS-Université
9 d'Orléans, 3A avenue de la recherche scientifique, Orléans, France

10 ²Laboratoire des Sciences du Climat et de l'Environnement (LSCE), UMR CEA-CNRS-UVSQ, IPSL,
11 Université Paris-Saclay, CEA Saclay 701, Gif-sur-Yvette, France

12 ³Laboratoire d'Aérodologie, Université de Toulouse, CNRS, UT3, Toulouse, France

13 ⁴Department of Meteorology and Bolin Centre for Climate Research, Stockholm University,
14 Stockholm, Sweden

15 ⁵Centre National de Recherches Météorologiques (CNRM), UMR Météo-France-CNRS, OMP, Météo-
16 France, Toulouse, France

17 ⁶Centre National d'Etudes Spatiales (CNES), 18 Avenue Edouard Belin, Toulouse, France

18 ^anow at MeteoModem company, Chemin du Moulin, Ury, France

19 ^bnow at CNRM⁵

20
21
22

23 **Abstract.** Mineral dust from arid areas is a major component of the global aerosol and has strong
24 interactions with climate and biogeochemistry. As part of the Chemistry-Aerosol Mediterranean
25 Experiment (ChArMEx) to investigate atmospheric chemistry and its impacts in the Mediterranean
26 region, an intensive field campaign was performed from mid-June to early August 2013 in the
27 western basin including in situ balloon-borne aerosol measurements with the Light Optical Aerosol
28 Counter (LOAC). LOAC is a counter/sizer that provides the aerosol concentrations in 19 size classes
29 between 0.2 and 100 μm , and an indication of the nature of the particles based on dual angle
30 scattering measurements. A total of 27 LOAC flights were conducted mainly from Minorca Island
31 (Balearic Islands, Spain) but also from Ile du Levant off Hyères city (SE France) under 17 Light
32 Dilatable Balloons (meteorological sounding balloons) and 10 Boundary Layer Pressurized Balloons
33 (quasi-Lagrangian balloons). The purpose was to document the vertical extent of the plume and the
34 time-evolution of the concentrations at constant altitude (air density) by in situ observations. LOAC
35 measurements are in agreement with ground-based measurements (lidar, photometer), aircraft
36 measurements (counters), and satellite measurements (CALIOP) in case of fair spatial and temporal
37 coincidences. LOAC has often detected 3 modes in the dust particle volume size distributions fitted
38 by lognormal laws at roughly 0.2, 4 and 30 μm in modal diameter. Particles larger than 40 μm were
39 observed, with concentrations up to about 10^{-4} cm^{-3} . Such large particles were lifted several days
40 before and their persistence after transport over long distances is in conflict with calculations of dust
41 sedimentation. We did not observe any significant evolution of the size distribution during the
42 transport from quasi-Lagrangian flights, even for the longest ones (~ 1 day). Finally, the presence of
43 charged particles is inferred from the LOAC measurements and we speculate that electrical forces
44 might counteract gravitational settling of the coarse particles.

45
46

47 **1. Introduction**

48
49
50
51

Mineral dust from arid and semi-arid areas is a major component of the global aerosol and has long
been recognized to have strong interactions with climate and biogeochemistry (e.g., Buat-Ménard
and Chesselet, 1979; Martin et al., 1991; Swap et al., 1992; Duce, 1995; Alpert et al., 1998;



52 Mahowald et al., 2009; Maher et al., 2010; Liu et al., 2011; Mahowald et al., 2011; Choobari et al.,
53 2014; Li et al., 2016). Desert dust aerosol is of particular interest in the Mediterranean region where
54 it is frequently observed in high concentrations in the troposphere, being a major component of
55 surface PM_{10} (Pey et al., 2013; Rea et al., 2015), aerosol optical depth (Moulin et al., 1998; Gkikas et
56 al., 2013; Nabat et al., 2013), atmospheric deposition (Pye, 1992; Vincent et al., 2016), affecting the
57 regional air quality (Querol et al., 2009), atmospheric thermodynamics (e.g. Alpert et al., 1998;
58 Chaboureaud et al., 2011), radiative budget and climate (e.g., Nabat et al., 2012, 2015a, 2015b),
59 precipitation chemistry (Chester et al., 1996; Loÿe-Pilot et al., 1986; Avila and Rodà, 2002), soil
60 formation (Nihlén et al., 1995), and biogeochemistry of forest ecosystems (Avila and Peñuelas, 1999),
61 oligotrophic lakes (Morales-Baquero et al., 2006; Reche et al., 2009) and marine surface waters
62 (Guerzoni et al., 1999; Herut et al., 1999; Guieu et al., 2014).

63 Most studies to characterize airborne dust particles transported long-range were performed
64 with satellite remote sensing and/or surface in-situ and remote sensing instruments (counters,
65 particles samplers, lidars, photometers...). Some aircraft observations were also conducted in situ
66 inside dust plumes, but they are expensive and scarce (e.g., Schmid et al., 2000; Dulac and Chazette,
67 2003; Reid et al., 2003a; Formenti et al., 2008; Weinzierl et al., 2009; Denjean et al., 2016). In
68 particular, there is some debate in the literature on the very-long distance transport of coarse soil
69 dust particles ($>10 \mu\text{m}$ in diameter). It has been shown that a coarse mode at about $14 \mu\text{m}$ in
70 diameter is produced by sandblasting of arid soils by saltating sand grains (Alfaro et al., 1998; Alfaro
71 and Gomes, 2001). Furthermore, d'Almeida and Schütz (1983) report that African dust storm
72 conditions produce a dust particle volume size distribution extending up to several tens of μm with a
73 highly variable 'giant' mode around $60 \mu\text{m}$ in diameter. The modified Stokes-Einstein law indicates
74 that steady state gravitational settling velocities (V_g) of particles in air are proportional to the
75 squared particle diameter (Stokes, 1851). For a particle density of 2.5 g cm^{-3} typical of soil dust, V_g
76 reaches 1 cm s^{-1} between 11 and $12 \mu\text{m}$ and 10 cm s^{-1} between 36 and $37 \mu\text{m}$, i.e. 860 and
77 8600 m d^{-1} , respectively (Foret et al., 2006). Those giant particles are therefore expected to fall and
78 control the dust deposition flux within the first 1000 km of transport from their source (Schütz et al.,
79 1981). However, there are evidences of Aeolian dust transport and sedimentation in the ocean up to
80 $10\,000 \text{ km}$ away from source regions in the tropical Atlantic (Prospero et al., 1970; Carder et al.,
81 1986) and Pacific (e.g. Betzer et al., 1988; Middleton et al., 2001; Jeong et al., 2014). Thus, there was
82 a need of a new strategy for multiplying in-situ measurements of the dust particle size distribution
83 during the transport of dust plumes. This was done for the first time in this study during African dust
84 transport events above the western Mediterranean, deploying optical particle counters both below
85 sounding balloons that crossed vertically the dust plume, and aboard drifting balloons that remained
86 at constant altitude for quasi-Lagrangian measurements within the atmospheric dust layer.

87 The Chemistry-Aerosol Mediterranean Experiment (ChArMEx; <http://charmex.lscce.ipsl.fr>) is
88 an international research initiative to investigate atmospheric chemistry in the Mediterranean region
89 and its impacts on air quality, marine biogeochemistry and the regional climate. Within the project, a
90 large regional field campaign was performed from mid-June to early August 2013 with intensive
91 airborne measurements including in situ balloon-borne aerosol (Mallet et al., 2016) and ozone
92 (Gheusi et al., 2016) measurements. The observations were conducted during the dry season over
93 the western and central Mediterranean basins. During the first special observation period (SOP)
94 entitled Aerosol Direct Radiative Forcing on the Mediterranean Climate (ChArMEx/ADRIMED SOP-1A)
95 from mid-June to early July, the focus was on aerosol-radiation measurements and their modelling
96 (Mallet et al., 2016). During the second SOP entitled Secondary Aerosol Formation in the
97 Mediterranean (ChArMEx/SAFMED SOP-1B) from mid-July to early August, the focus was on
98 atmospheric chemistry (Zannoni et al., 2017).

99 The present paper focuses on balloon-borne measurements conducted over the western
100 Mediterranean during desert dust episodes encountered during this summer campaign with the new
101 Light Optical Aerosol Counter (LOAC), an optical particle counter/sizer (OPC). Renard et al. (2016a
102 and b) present the LOAC instrument and preliminary results from some flights analysed here with
103 more details. In the following, we first briefly summarize the instrument principle and performances



104 and we describe the different sounding and drifting balloon flights performed in summer 2013
105 (section 2). Results on the particle size-segregated dust concentration are then presented, first in
106 terms of vertical distribution (section 3), and second in terms of temporal evolution at constant
107 altitudes (section 4). We then discuss dust particle sedimentation aspects (section 5) and
108 speculations about electrically charged dust particles (section 6), and finally conclude (section 7).

109

110

111 2. Experimental strategy

112

113 This study is based on the LOAC instrument (Figure 1), a light OPC described and characterized by
114 Renard et al. (2016a). Briefly, the instrument provides aerosol particle concentration measurements
115 within 19 size classes in the 0.2–100 μm diameter size range, and an estimate of the typology of
116 aerosols based on dual angle measurements. LOAC can be carried by all kinds of balloons (Renard et
117 al., 2016b). The gondola weight, including the instrument, the batteries (alkaline or lithium) and the
118 telemetry system, is of about 1.0 kg, for an electric consumption of 3 W. Aerosols are sucked in by a
119 small pump in order to pass through a red laser diode beam. In general, the light scattered by the
120 particles depends on both the size and refractive index of the particles. To separate these two
121 parameters, LOAC uses an original concept described in Renard et al. (2016a). Measurements are
122 performed at 2 scattering angles: the first one is close to forward scattering at around 12° where the
123 light scattered (diffracted) by non-spherical particles is controlled by the size of the particles (Lurton
124 et al., 2014); the second one is around 60° , where the scattered light is strongly dependent on the
125 refractive index of the particles (e.g., Weiss-Wrana, 1983; Renard et al., 2010; Francis et al., 2011).
126 The 12° channel is used to retrieve the size distribution independently of the nature of the particles,
127 and the combination of the 12° and 60° channels is used to derive the “LOAC speciation index” that
128 informs on the typology or dominant nature of aerosol particles in each size range, based on a
129 laboratory calibration conducted with particles of well-known nature. Figure 2 presents the reference
130 “speciation zones” obtained in laboratory and an example of LOAC speciation index obtained during
131 ambient air measurements inside a Saharan dust plume on 18 June above Minorca (Spain) at an
132 altitude of 3.1 km.

133 As described by Renard et al. (2016a), the measurement uncertainty on the total aerosol
134 concentration is $\pm 20\%$ for concentration values greater than 1 particle per cm^3 (for a 10-min
135 integration time). In contrast, the uncertainty is up to about 60% for concentration values smaller
136 than 10^{-2} particle per cm^3 . In addition, the uncertainty in size calibration is $\pm 0.025 \mu\text{m}$ for particles
137 smaller than $0.6 \mu\text{m}$, 5% for particles in the $0.7\text{--}2 \mu\text{m}$ range, and 10% for particles larger than $2 \mu\text{m}$.
138 Following coincidences, the measurement accuracy for submicronic particles could be reduced in a
139 strongly turbid case when the concentration of particles larger than $3 \mu\text{m}$ exceeds a few particles per
140 cm^3 .

141 During the ChArMEx summer 2013 campaign, the LOAC gondolas were carried by two types
142 of balloon: the Light Dilatable Balloon (LDB), a meteorological sounding balloon of about 1 kg, and
143 the Boundary Layer Pressurized Balloon (BLPB), a drifting balloon of about 2.5 m in diameter.
144 Pictures of the respective gondolas can be found in Renard et al. (2016b).

145 The LDB allows many flights from various places, and the gondola may generally be retrieved
146 after landing (if not at sea). Measurements were conducted during the ascending phase of the
147 balloon, at a speed of $3\text{--}6 \text{ m s}^{-1}$. The inlet that collects aerosols was oriented toward the sky. The low
148 flow rate ($\sim 1.7 \text{ L min}^{-1}$) of the sampling pump yields sub-isokinetic sampling conditions that could
149 tend to oversample large particles (Renard et al., 2016a). The highest altitude reached by LOAC was
150 37 km, although in this study we will only consider the tropospheric part below 8 km in altitude (see
151 Chane Ming et al. (2016) for an analysis of upper troposphere and stratosphere observations). The
152 LOAC measurements, integrated every 10 s, are sent to ground in real-time by the on-board
153 telemetry. To increase the measurement accuracy during the LDB ascent, the 10-s concentration
154 values are averaged over a 1-min period, which provides a vertical resolution of about 300 m.



155 The BLPB, after its ascending phase, follows a near-Lagrangian trajectory, remaining in the
156 same air mass during its trajectory in the lower atmosphere (Ethé et al. 2002; Gheusi et al., 2016;
157 Doerenbecher et al., 2016). Its float altitude was prescribed before the flight (in the 400-3500 m
158 range) by adjusting the balloon density with the appropriate mixture of air and helium. The altitude
159 was chosen to fly within dust layers, based on a LDB flight and/or aerosol lidar measurements
160 performed just before the launch. At the float level, the horizontal speed of the drifting balloon
161 relatively to ambient air is close to zero, thus the particle sampling efficiency should be close to
162 100%. The integration time was chosen between 1 and 20 min, due to the low telemetry rate for the
163 downlink through the Iridium satellite communication system. The duration of the flights varied from
164 several hours to more than one day. Also, LOAC was sometimes temporarily shut down after a
165 session of measurements to save up on-board energy. For safety reasons, the authorized flight area
166 was restricted to the sea (including islands).

167 Table 1 and Table 2 provide the conditions of measurements for LDB and BLPB flights
168 performed during the ChArMEx campaign, respectively. Seventeen LDB flights and 10 BLPB flights
169 were successfully performed during desert dust transport events, most of them launched from
170 Minorca, the easternmost Balearic Island, Spain (latitude 39.88°N, longitude 4.25°E) from 15 June to
171 2 July, and a few from Ile du Levant, off Hyères city near the coast of south eastern France (latitude
172 43.02°N, longitude 6.46°E) from 27 July to 4 August (Figure 3). Those dust events were identified by
173 near-real time (NRT) model and remote sensing products collected operationally by the ChArMEx
174 Operation Centre web server (<http://choc.sedoo.fr>) where quick-looks were available. The main NRT
175 remote sensing aerosol products were provided by 4-hourly observations from MSG/SEVIRI. The
176 aerosol optical depth (AOD) at 550 nm (AOD₅₅₀) product is based on Thieuleux et al. (2005). In
177 addition, we operated a calibrated ground-based CIMEL AERONET sun-photometer that provided
178 AOD at 7 wavelengths from 340 to 1020 nm during daytime at the nearby station of Cap d'en Font on
179 Minorca Island (39.826°N, 4.208°E; <http://aeronet.gsfc.nasa.gov>) where an aerosol and water vapour
180 Raman lidar (WALI) with polarisation measurements was also in continuous operation (Chazette et
181 al., 2016). The balloon launch site and the lidar and photometer station were distant by about 10 km.
182 The confirmation of the occurrence of mineral dust plumes was possible from the LOAC-derived
183 typology of aerosol particles with the LOAC speciation index falling inside the "mineral zone" (Renard
184 et al., 2016a and b).

185 In case of a strong dust event, the measurement strategy was to perform two LDB flights per
186 day, and two simultaneous BLPB flights drifting at different altitudes within the dust plume (twin
187 flights). The flight altitudes were chosen following real-time indications from the nearby lidar. This
188 strategy was conducted during a relatively long dust event from 15 to 19 June, with 9 LDB flights and
189 3 twin BLPB flights on June 15, 16, and 19. The MODIS satellite observations indicate that the mean
190 AOD was of about 0.25 during this period. The dust started to appear over the Alboran Sea on June
191 12. The daily average AOD derived from MSG/SEVIRI over the western Mediterranean basin from
192 June 15 to 18 is mapped in Figure 4. It shows the arrival of the plume from the South-West with a low
193 AOD over Minorca on June 15, its extension to the North and North-East on June 16 and 17 with a
194 maximum extent of the plume over the basin on June 17, its reinforcement along a North-South axis
195 on June 18 with the largest AOD values around the Balearic Islands. On June 19 (not shown) Minorca
196 was on the western edge of the plume that shifted eastward.

197 The WALI lidar provides the vertical extent, the time-evolution and an estimate of the nature
198 of the particles during this event. Figure 5 shows times series of products from the lidar from late
199 June 15 to the end of June 17. The high extinction areas below 2.5 km until June 16, 13:00 are not or
200 weekly depolarizing. Chazette et al. (2016; see their Figure 7) could infer from those data that the
201 dominant aerosol was of marine nature around 500 m in altitude within the atmospheric boundary
202 layer, dust over 2.5 km, and pollution-related in between during the night of 15 to 16 June.

203 Five LDB flights were also conducted during the 28 June-2 July period. On 27-29 June, the
204 Minorca region was affected by turbid air masses arriving from the North-West (Chazette et al.,
205 2016). Ancellet et al. (2016) identified long-range transport of forest fire smoke from different areas
206 in North America (Canada and Colorado) and of African dust back from the western tropical Atlantic.



207 Their Flexpart model simulations indicate that over Minorca, Canadian smoke aerosols dominated
208 below 3 km on June 28 late afternoon, when dust dominated above 4 km and Colorado smoke
209 aerosols were abundant above 5 km. Satellite-derived AOD shows that starting on June 29, a new
210 dust plume from northwestern Africa with high AOD emerged from the Atlantic and Mediterranean
211 coasts of Morocco. The plume extended a bit to the North and further East over the sea during the
212 following days but remained confined to the southernmost part of the basin, with moderate AODs
213 and some dust over Minorca on 2 July 2 (Chazette et al., 2016). A BLPB flight was conducted on 2
214 July; the mean MODIS AOD was of 0.15 during this period. Lidar data indicate that dust dominated
215 between about 2 and 4.8 km in altitude (Chazette et al., 2016). The aerosol in lower layers could not
216 be typified.

217 Two other LDB flights were conducted from the Ile du Levant during a dust event on 27-28
218 July, with a mean MODIS AOD of 0.35. Finally, 2 LDB flights and one BLPB flight were conducted
219 during a last dust event on 3-4 August, with a mean MODIS AOD of 0.25.

220 The 27-28 June and the 2-3 July BLPB flights were the longest ones, with duration of about 1
221 day. Day-night transitions were thus encountered, leading to a decrease in float altitude during the
222 night of more than 100 m. Finally, the slow speed ascent of the 19 June and 3 August BLPBs allowed
223 us to obtain two additional fine-resolution vertical profiles in the lower troposphere.

224 From all those flights, it is possible to study the vertical extent of dust plumes and the
225 temporal evolution of the dust particle size-segregated concentration at a given altitude during
226 transport. In particular, LOAC data can be used to determine the concentration of large particles
227 dominating the mass of desert dust transported and their deposition flux (e.g. Arimoto et al., 1985;
228 Dulac et al., 1987, 1992a and b; Foret et al., 2006).

229
230

231 3. Vertical profiles and particle size distributions of the observed dust plumes

232

233 The main desert dust event observed during the ChArMEx/ADRIMED campaign lasted five days from
234 15 to 19 June as presented above (Figure 4). Figure 6 presents the vertical distribution of the 19 size
235 class number concentrations, from the 9 LDB flights performed during that period. It shows that the
236 dust plume was heterogeneously distributed in the free troposphere allowing for several local
237 concentration maxima along the vertical and extended up to 7 km on the evening of 18 June. For
238 comparison, Figure 7 presents measurements during a dust-free flight from Aire sur l'Adour, France
239 (43.706°N, -0.251°E) on 14 August 2014, with no significant local enhancement and the absence of
240 large particles.

241 All these flights, including a BLPB flight on 19 June morning when LOAC performed
242 measurements during the balloon ascent, were conducted concurrently to the nearby aerosol lidar
243 measurements (Chazette et al., 2016). The time of the first 5 LDB flights are presented on the WALL
244 lidar time-height cross-sections on June 16-17 with arrows marking. The LOAC aerosol number
245 concentration in the 0.2-100 μm range was converted to aerosol extinction using the Mie scattering
246 theory, assuming spherical dust particles, to be compared to the lidar extinction data at 350 nm. The
247 refractive index was set to 1.53-i0.0025, which corresponds to the mean value determined by
248 Denjean et al. (2016) for the Saharan dust plume events documented during the summer 2013
249 ChArMEx campaign. This approach suffers from three approximations: i) the contribution of the
250 smallest particles is unknown, leading to an underestimate of the calculated aerosol extinctions, ii)
251 the grains are considered as spherical while they are not and iii) the refractive index of the grains is
252 not always well known. In fact, the grains are irregular in shape and their refractive index can vary,
253 depending on their composition and their origin, which potentially increases the uncertainty on the
254 calculation of the aerosol extinction. Also, extinction calculations are highly sensitive to the size of
255 the particles: the uncertainty in the LOAC particle size determination can produce a 50% uncertainty
256 on the derived extinctions. Thus, the error bars on the LOAC-derived extinctions are calculated
257 considering both concentration and size uncertainties. Weinzierl et al. (2009) report that accounting
258 for the non-sphericity of dust particles might yield a small reduction of up to 5% in extinction



259 computations based on the dust particle size distribution. Figure 8 presents the tropospheric vertical
260 profiles of the LOAC and concurrent WALI lidar aerosol extinction observed during the 15-19 June
261 dust event over Minorca. Taking into account the uncertainties associated to the different
262 instruments, the overall aerosol extinction values can be regarded as in the same order of
263 magnitude, and even often in good agreement. LOAC and WALI have captured similar vertical
264 structures around half the time. The remaining discrepancies could be due to inaccurate size
265 determination by LOAC, and to the distance between different observations of inhomogeneous dust
266 plumes.

267 Three other dust events were documented with the LOAC instrument as illustrated in
268 Figure 9. The 28 June-2 July event was not very intense, while the 27-28 July and 3-4 August events
269 were stronger. Similarly to the mid-June event, the dust plumes extended up to an altitude of 6 km
270 and were not homogeneous in the vertical.

271 Good spatial and temporal coincidences occurred between LOAC measurements and Cloud-
272 Aerosol Lidar with Orthogonal Polarization (CALIOP on board the CALIPSO satellite) remote sensing
273 measurements for two events: on 29-30 June above Minorca (Spain) and on 3 August above Ile du
274 Levant (France). The LOAC measurements on 29-30 June were between 23:45 and 01:50 UT while the
275 CALIOP measurements were at 01:56 on 30 June. The LOAC measurements on 3 August were
276 between 11:15 and 12:15 while the CALIOP measurements were at 12:49. We used CALIOP version
277 4.10 level-2, 532 nm aerosol extinction data in the troposphere (e.g., Winker et al., 2009). The data
278 have a horizontal resolution of 5 km and a vertical resolution of 60 m. Aerosol extinction values have
279 a detection threshold of about 0.01 km^{-1} . The nature of aerosol particles and cloud droplets retrieved
280 in CALIOP observations is given by the CALIOP vertical feature mask algorithm (Omar et al., 2009). To
281 perform the comparison with CALIOP aerosol extinction data, the LOAC aerosol extinctions are
282 calculated at 532 nm from the measured size distribution using the mineral dust refractive index as
283 presented above. Lidar WALI extinctions are also available for the 29 June at around 22:30.

284 Figure 10 presents the comparison between LOAC, CALIOP and WALI aerosol extinctions.
285 During the 29-30 June night, the 3 instruments show that the plume extended from the ground to an
286 altitude of 2.5 km. Although the general trend is in good agreement for the 3 instruments, local
287 discrepancies are present in the vertical extinction profiles, possibly due to the temporal and spatial
288 variability of the plume. LOAC seems to indicate a mixture of mineral dust and carbonaceous
289 particles whereas CALIOP reports polluted continental/smoke particles (but the identification by
290 CALIOP is difficult due to the weakness of the signal). On 30 June at mid-day, the plume had almost
291 disappeared and the LOAC aerosol extinction values are below the detection threshold of CALIOP.

292 During the 3 August dust event, LOAC observations reveal that the plume extended from 2 to
293 6.5 km. CALIOP captured all the dust plume in very good agreement with LOAC, and the two
294 instruments identified the same nature of mineral dust particles. Another LOAC profile was obtained
295 in the morning of 3 August at about 06:30 UT, during a BLPB ascent up to its float altitude at 3 km (in
296 blue in Figure 10). The two LOAC measurements are in very good agreement in the 2-3 km altitude
297 range. Below 2 km, the 2 flight measurements show that the detected typologies are dominated by
298 carbonaceous particles (likely anthropogenic aerosols). The strong temporal variability in particle
299 concentrations below 2.2 km is therefore not related to the dust plume.

300 An ATR-42 aircraft flight was conducted close to Minorca (50 km apart) during dusty
301 conditions in the morning of 16 June, at the same time of two LOAC balloon flights (LBD and BLBP).
302 The aircraft probed the dust layer in the 2.5-4 km altitude range. The instrumentation installed on
303 board the aircraft is described in detail in Denjean et al. (2016). The aerosol size distribution was
304 determined from an optical particle counter GRIMM 1.129 (nominal size range 0.25-32 μm), an Ultra
305 High Sensitivity Aerosol Spectrometer (UHSAS; 0.04-1 μm) and a Forward Scattering Spectrometer
306 Probe FSSP-300 (0.28-20 μm). The UHSAS and FSSP are wing-mounted instruments, whereas the
307 GRIMM installed inside the cabin received ambient air collected through an isokinetic inlet and
308 tubing with a cut-off diameter of 12 μm (Denjean et al., 2016). Figure 11 presents the comparison of
309 the size distributions measured by the 2 LOACs and the 3 aircraft counters at the maximum
310 concentration level of the dust plume (2.5-4 km; see Figures 5 and 6). The integration from 2.5 to



311 4 km of the LDB LOAC signal provides a better signal to noise ratio and a better sensitivity to the less
312 numerous large particles ($>15\ \mu\text{m}$) that are hardly detected with short integration times. Globally, all
313 the instruments are in good agreement for the submicronic particles and for the coarse mode at 2-
314 $3\ \mu\text{m}$; the small discrepancies can be due to the difference in the respective measurement locations
315 and to the different measurement methods of the various instruments, although they were all
316 calibrated. The FSSP shows larger concentrations for particles larger than $2\ \mu\text{m}$ in diameter than
317 other instruments (Figure 11). Reid et al. (2003b) discuss that the FSSP measurement principle tends
318 to produce some oversizing of coarse particles and also shows particle concentrations as high as
319 twice those measured by a Passive Cavity Aerosol Spectrometer Probe (PCASP) in their overlapping
320 particle diameter range ($1.5\text{-}3\ \mu\text{m}$). This could explain such a shift in our dataset. It is worth noting
321 that the two LOACs, the FSSP and the GRIMM (despite the $12\ \mu\text{m}$ cut-off of its sampling inlet) all
322 report particle concentrations larger than $10^{-3}\ \text{cm}^{-3}$ around $20\ \mu\text{m}$ in diameter. Both LOAC flights have
323 detected similar concentrations of particles in the channels larger than $22\ \mu\text{m}$ in diameter. Although
324 the GRIMM counter on board the ATR42 aircraft could sense particles up to $32\ \mu\text{m}$, it did not report
325 such large grains, most probably because of the difficulty to collect and carry them up to the
326 instrument inside the aircraft cabin.

327 In Figure 12, the LOAC-derived size distributions were converted to volume concentrations
328 assuming spherical particles, using the mean volume diameter of each size class (Renard et al.,
329 2016a), and integrated over the whole vertical. The LOAC volume size distribution is compared to
330 that derived from the AERONET remote-sensing photometer. According to Dubovik and King (2000)
331 AERONET retrievals are limited to particles smaller than $30\ \mu\text{m}$ and are not very sensitive to the
332 largest particles. Both LOAC and AERONET volume size distributions are in very good agreement in
333 the $0.2\text{-}20\ \mu\text{m}$ size range, although the LOAC measurements show the presence of a third mode of
334 particles larger than $20\ \mu\text{m}$. Since the concentration of these large particles is low, the analysis of this
335 mode from measurements during LBD flights is limited. Long duration measurements performed at
336 constant altitude using the LOAC instrument on BLPB gondola with much longer measurement
337 integration time are better adapted to evaluate the concentration of these large particles and to
338 discuss this third, giant size mode.

339

340

341 **4. Temporal evolution of the dust aerosol concentration and particle size distribution at** 342 **constant altitudes**

343

344 Figure 13 presents results from the BLPB flights performed inside dust plumes and Table 2 details the
345 conditions of measurements. Twin flights were performed on 16 June at the lower edge and in the
346 middle of the dust layer, on 17 June well inside the maximum concentration of the plume, and on 19
347 June at the minimum and maximum concentrations of the plume. On 27 and 28 June, flights were
348 performed in the upper edge of the plume. Finally, on 2 July and 3 August flights were conducted at
349 the maximum concentrations of the plume. It can be noticed that the 27 June and 2 July flights lasted
350 for about one day, with a day-night-day transition. In these cases, the altitude of the balloon is
351 slightly lower (from 100 to $200\ \text{m}$) at night than during the day due to the cooling of the balloon gas
352 and associated loss in buoyancy, so the night-time and daytime measurements were not conducted
353 in exactly the same air mass.

354 The LOAC aerosol concentration values obtained during the BLPB ascent on 19 June are in
355 good agreement with the LBD ascent measurements conducted at the same time (Figure 8, lower
356 right panel). In particular, LOAC has well captured the vertical variation of the dust plume
357 concentrations, with a local minimum at an altitude of $2\ \text{km}$.

358 During most of the flights, particles larger than $40\ \mu\text{m}$ in diameter (last LOAC channel) were
359 detected. The concentration of these particles depends mainly on the intensity of the event, but the
360 highest concentration was detected in the free troposphere on 19 June, with 10^{-4} particles per cm^3 at



361 an altitude of 3.3 km. It can be noticed that concentrations of 10^{-3} particles per cm^3 were detected at
362 ground at the same date, as shown in Figure 6.

363 The dust particle volume size distributions were computed by integrating data over more
364 than a minute at a constant altitude. The mean diameter of the last channel was assumed to be 50
365 μm , although the size range is 40-100 μm , because the concentrations strongly decrease with size
366 and most of the particles thus have a diameter close to the lower limit of the size class. Those volume
367 distributions were then fitted with a 3-mode log-normal model using a least-square procedure. The
368 three fitted volume modal diameters (D_m) have been found at about 0.2, 4 and 30 μm as illustrated
369 in Figure 14. Note, however, that only the decreasing part of the first (small) mode is captured by
370 LOAC and the corresponding modal diameter could therefore be misestimated. There is also some
371 uncertainty on the third (large) mode related to the assumed upper limit of the measurement size
372 range and to the possible under-sampling of the upper tail of the size distribution; thus this mode
373 value may be a lower limit.

374 Figure 15 shows the evolution of D_m for the three modes fitted from the 3 pairs of BPCL
375 LOAC data obtained during the 15-19 June dust event. BLPB flights lasted between 6 and 11 hours.
376 No significant temporal trend can be pointed out for D_m , meaning that the size distribution remains
377 almost constant over hours. Thus, it seems that no significant sedimentation has been detected
378 during the flights at quasi-constant altitude even for the very coarse mode at about 30 μm in
379 diameter.

380 Table 3 gives the values of D_m for the 3 modes at float altitude for the 6 BPCL flights in dust
381 layers during the 16-19 June event; the average values are 0.26, 3.7 and 30.4 μm , respectively.
382 Values for the 3 modes are very comparable from one balloon to the other with a small variability of
383 about 15%, likely not significant given the uncertainties of the fitting. The flights inside the other dust
384 events confirm the presence of large particles in a giant mode at about 30 μm in diameter.
385 Nevertheless, some variations in aerosol concentrations often occurred. They are due to changes in
386 the balloon altitude during the day-night transition for the 27-28 June and the 2-3 July flights, to a
387 non-constant altitude for the 28 June flight, and to a slow ascent during the 3 July flight. These
388 variations of concentration are thus probably related to vertical variations of the dust plume layer.
389 Indeed, lidar profiles from Minorca show a strong vertical structuration of aerosol layers (Chazette et
390 al., 2016) that could be associated with significant differences in aerosol composition, concentration
391 and size distribution. Hamonou et al. (1999) first documented the multi-layered African dust
392 transport over the Mediterranean basin with variable source regions of mineral dust particles found
393 in different layers of the plume.

394 The presence of the third, very coarse mode with D_m of the order of 30 μm may be related
395 to the existence of a mode in desert dust aerosols: a value of the same order ($D_m=42.3 \mu\text{m}$) is
396 assumed in the model of background desert dust aerosol of Jaenicke (1987). Observations of a very
397 coarse mode are also reported by Weinzierl et al. (2009): particles larger than 20 μm were detected
398 in nine out ten cases of 49 pure dust layers observed in altitude over southern Morocco with wing-
399 mounted airborne optical particle counters. In 20% of the cases, particle sizes equal or larger than 40
400 μm and up to 80 μm were detected (with a detection limit of 10^{-2}cm^{-3}). They report an average
401 volume median diameter of the coarse mode of $15.5 \pm 10.9 \mu\text{m}$ near dust source region and a
402 maximum value larger than 60 μm in a case of strong convection. The better sensitivity of LOAC may
403 explain why we report more systematically a coarse mode of dust particles above 20 μm in diameter.
404 However, the persistence of such large particles, lifted several days ago, and their transport above
405 the Mediterranean basin is not well understood given their large theoretical settling velocity.

406

407

408 5. Discussion related to dust sedimentation

409

410 According to the Stoke's approximation that equates the effective weight of spherical
411 particles and the viscous resistance of the fluid through which it moves (Stokes, 1851), the



412 gravitational settling velocity V_g of dust particles is proportional to the square of their diameter.
413 Assuming a classical density value of 2.5 g cm^{-3} for spherical dust particles (Dulac et al., 1989; Zender
414 et al., 2003; Linke et al., 2006), V_g is thus about 0.076, 0.19, 0.76, 3.0, 6.8, and 19 cm s^{-1} for particles
415 of 1, 5, 10, 20, 30 and $50 \mu\text{m}$ in diameter, respectively, implying a downward transport ranging from
416 about 66 to $16\,400 \text{ m d}^{-1}$. Particles larger than $12.3 \mu\text{m}$ have a sedimentation velocity larger than
417 $1\,000 \text{ m d}^{-1}$. This is supposed to yield a quick segregation and a rapid evolution of the dust particle
418 size distribution in the first days (and even hours) of transport after lifting from the dust source
419 region (e.g., Schütz et al., 1981; see also Figure 1 in Foret et al., 2006). Dust-loaded air masses
420 transported northward from Africa above the marine atmospheric boundary layer in the western
421 Mediterranean are known to be associated with warm fronts and to experience a significant upward
422 synoptic movement (Prodi and Fea, 1979; Reiff et al., 1986). Dulac et al. (1992a and b) report that
423 during a typical summer dust episode the turbid air mass ascending vertical velocity was on average
424 of the order of 1.5 to 1.8 cm s^{-1} during 4 days, i.e. was more than compensating the average
425 deposition velocity of the bimodal dust particle size distribution observed in Corsica during this
426 event, with 2 modes at 2 and $13 \mu\text{m}$. This is not enough, however, to explain the relatively constant
427 dust particle size distribution observed during BPCL flights: accounting for an average upward air
428 mass vertical velocity of 1.5 cm s^{-1} that would counteract gravitation, a 4-km thick dust layer should
429 anyway lose by sedimentation all particles larger than $30 \mu\text{m}$ in about 1 day.

430 According to Slinn (1983; eq. 160), the flux-mean deposition velocity ($\langle V_d \rangle$) of a lognormal
431 distribution of particles of modal diameter D_m and geometric standard deviation σ_g can be derived
432 from $\langle V_d \rangle = V_d(D_m) \sigma_g^{2 \ln(\sigma_g)}$. Using this formula, we can derive that the 3-fitted dust particle size
433 modes shown in Figure 14 have a respective gravitational settling velocity of about 0.0011, 0.50, and
434 8.1 cm s^{-1} , corresponding to a negligible downward transport by sedimentation of about 1 m d^{-1} for
435 the finest mode, but to 430 m d^{-1} for the intermediate mode, and as much as $7\,000 \text{ m d}^{-1}$ for the
436 largest one. Figure 13 does not show any significant systematic evolution of the concentration of the
437 different modes. New particles sedimenting from turbid layers above the balloon might compensate
438 for the sedimentation of particles from the intermediate coarse mode with D_m of about $4 \mu\text{m}$ during
439 our 1-d or less balloon flight times. However, we should definitely observe a significant decrease in
440 the concentration and median size of the very coarse mode with $D_m \approx 30 \mu\text{m}$. Figure 15 does not
441 show any evidence of a decrease in the very coarse mode median diameter.

442
443

444 6. Indirect detection of possible charged particles

445

446 Laboratory tests have shown that the LOAC photodiode and electronics are sensitive to
447 electromagnetic fields, as those generated by radio telemetry, by strong atmospheric electric activity
448 (e.g., during thunderstorms), and even by an electrical bay. In these cases, the electronic noise and
449 the electronic offset both increase. The offset also increases with increasing ambient temperature.

450 LOAC performs measurements of the electronic noise and offset every 15 min when the light
451 source is switched off (Renard et al., 2016a). During a typical LDB flight, the LOAC electronic offset
452 slightly decreased with altitude due to the decreasing temperature encountered during the balloon
453 ascent. In contrast, an offset increase correlated to the increase in dust particle concentration was
454 detected for 5 flights inside a dust plume (Figure 16). It seems that increases in the amplitude of the
455 offset and in concentration were correlated. No conclusion can be derived from the other flights
456 inside the plumes, since no offset control was done close to the maximum in dust concentration.
457 These offset increases may be related to the presence of local strong electromagnetic fields inside
458 the plume, although it is not possible to retrieve their strength with such kinds of measurements. It is
459 known that the aerosol generation from both mineral dust powders (e.g., Johnston et al., 1987;
460 Forsyth et al., 1998) and arid soils (e.g. Ette, 1971; Farrell et al., 2004; Sow et al., 2011) produces
461 charged particles, and that electrical charges in sandstorms perturb telecommunication
462 transmissions (e.g. Li et al., 2010 and references therein). The presence of electric field in dust



463 aerosol layers was indeed proposed by Ulanowski et al. (2007) to explain the alignment of non-
464 spherical particles and polarization effects in a dust plume over the Canary Islands. Nicoll et al. (2011)
465 also report charged particles within Saharan dust layers with two balloon soundings performed
466 above Cape Verde Islands.

467 We suggest that electric forces within the dust layers could contribute maintaining in
468 levitation coarse particles that would otherwise expected to sediment down. Future balloon
469 campaigns with LOAC measurement in parallel with an adequate instrument retrieving accurately the
470 atmospheric electric field could consolidate these previous studies. This looks as an important
471 perspective to consider since the local electric field in dust plume might be at least partly responsible
472 for the non-sedimentation of large particles resulting in much longer transport than expected.

473

474

475 7. Conclusions

476

477 The in-situ LOAC balloon-borne measurements above the Mediterranean basin in summer 2013 have
478 allowed us to document both the vertical extent of the dust plumes and, for the first time to our
479 knowledge, the time-evolution of dust concentrations from several hours to one day in a quasi-
480 Lagrangian way at constant altitude. Whenever possible, LOAC observations were compared to the
481 measurements done by other platforms, like the ATR-42 aircraft which embarked various aerosol
482 counters, and a backscattering lidar located close to the balloon launching area. Given the limits and
483 uncertainties associated with each measurement system, the agreement was satisfactory, which
484 gave us confidence in the LOAC aerosol distributions. LOAC has often detected the presence of
485 particles larger than 40 μm , with concentrations up to 10^4 particles per cm^3 , and the fitting of
486 volume size distribution ended up in a coarse mode at 3-4 μm in diameter and a giant mode at about
487 30 μm . Such large particles should have been lifted several days before, and at least 1 000 km far
488 from our measurements. Their transport over such long distances, not expected from calculations of
489 dust particle sedimentation, is yet not well understood. Indeed, the gravitational settling velocity of
490 dust particles between 12 and 40 μm in diameter spans from almost 1 to more than 10 km per day.
491 An indirect evidence of the presence of charged particles has been derived from the LOAC
492 measurements and we therefore hypothesize that electric forces within the dust plume might limit
493 the sedimentation of the coarse dust fraction.

494 ChArMEx was a unique experiment involving a large set of ground-based and airborne
495 instruments. Since 2014, regular LDBs with LOAC are launched twice per month from Aire-sur-l'Adour
496 (South-West of France, 43.71°N, 0.25°W) to monitor the aerosol content from the troposphere to the
497 stratosphere. Dust events were already occasionally detected; they will be used to document other
498 dust events than those of summer 2013 with the same instrument, and to confirm the presence of
499 both the large particles and the charged particles thanks to new developments of the instrumental
500 payload.

501

502

503 **Acknowledgments.** The LOAC development project was funded by the French National Research
504 Agency's ANR ECOTECH. The balloon flights of the MISTRALS/ChArMEx campaign were funded and
505 performed by the French Space Agency CNES. The LOAC instruments are built by Environnement-SA
506 company; the balloon-borne gondolas are provided by MeteoModem company and by CNES for
507 sounding and drifting balloons, respectively. The numerous LOAC instruments used during the
508 campaign and the scientific and technical staff missions were funded with the support of CNES, INSU-
509 CNRS and ADEME. The SAFIRE team is acknowledged for the aircraft operation. The French
510 VOLTAIRE-LOAC Labex (Laboratoire d'Excellence ANR-10-LABX-100-01) also provided a couple of
511 LOAC instruments. The PHOTONS (<http://loaphotons.univ-lille1.fr/>) and AERONET
512 (<https://aeronet.gsfc.nasa.gov/>) teams are acknowledged for our sun-photometer calibration and
513 data processing, respectively. P. Chazette and J. Totems are acknowledged for lidar data from
514 Minorca. ChArMEx LOAC balloon and other measurements are available on the ChArMEx database



515 (<http://mistrals.sedoo.fr/ChArMEx/>). Finally, CALIOP data have been retrieved through the ICARE
516 Data Services and Center (<http://www.icare.univ-lille1.fr>).

517

518

519 References

520

521 Alfaro, S. C., and Gomes, L.: Modeling mineral aerosol production by wind erosion: Emission
522 intensities and aerosol size distributions in source areas, *J. Geophys. Res.*, 106, 18075–18084,
523 doi:10.1029/2000JD900339, 2001.

524 Alfaro, S. C., Gaudichet, A., Gomes, L., and Maillé, M.: Mineral aerosol production by wind erosion:
525 Aerosol particle sizes and binding energies, *Geophys. Res. Lett.*, 25, 991–994,
526 doi:10.1029/98GL00502, 1998.

527 Alpert, P., Kaufman, Y. J., Shay-El, Y., Tanré, D., da Silva, A., Schubert, S., and Joseph, J. H.:
528 Quantification of dust-forced heating of the lower troposphere, *Nature*, 395, 367–370,
529 doi:10.1038/26456, 1998.

530 Ancellet, G., Pelon, J., Totems, J., Chazette, P., Bazureau, A., Sicard, M., Di Iorio, T., Dulac, F., and
531 Mallet, M.: Long-range transport and mixing of aerosol sources during the 2013 North American
532 biomass burning episode: analysis of multiple lidar observations in the western Mediterranean
533 basin, *Atmos. Chem. Phys.*, 16, 4725–4742, doi:10.5194/acp-16-4725-2016, 2016.

534 Arimoto, R., Duce, R. A., Ray, B. J., and Unni, C. K.: Atmospheric trace elements at Enewetak Atoll: 2.
535 Transport to the ocean by wet and dry deposition, *J. Geophys. Res.*, 90, 2391–2408,
536 doi:10.1029/JD090iD01p02391, 1985.

537 Avila, A. and Peñuelas, J.: Increasing frequency of Saharan rains over northeastern Spain and its
538 ecological consequences, *Sci. Total Environ.*, 228, 153–156, doi:10.1016/S0048-9697(99)00041-8,
539 1999.

540 Avila, A. and Rodà, F.: Assessing decadal changes in rainwater alkalinity at a rural Mediterranean site
541 in the Montseny Mountains (NE Spain), *Atmos. Environ.*, 36, 2881–2890, doi:10.1016/S1352-
542 2310(02)00098-5, 2002.

543 Betzer, P. R., Carder, K. L., Duce, R. A., Merrill, J. T., Tindale, N. W., Uematsu, M., Costello, D. K.,
544 Young, R. W., Feely, R. A., Breland, J. A., Bernstein, R. E., and Greco, A. M.: Long-range transport of
545 giant mineral aerosol particles, *Nature*, 336, 568–571, doi:10.1038/336568a0, 1988.

546 Buat-Ménard, P. and Chesselet, R.: Variable influence of the atmospheric flux on the trace metal
547 chemistry of oceanic suspended matter, *Earth Planet. Sci. Lett.*, 42, 399–411, doi:10.1016/0012-
548 821X(79)90049-9, 1979.

549 Carder, K. L., Stewards, R. G., Betzer, P. R., Johnson, D. L., and Prospero, J. M.: Dynamics and
550 composition of particles from an Aeolian input event to the Sargasso Sea, *J. Geophys. Res.*, 91,
551 1055–1066, doi:10.1029/JD091iD01p01055, 1986.

552 Chaboureaud, J.-P., Richard, E., Pinty, J.-P., Flamant, C., Di Girolamo, P., Kiemle, C., Behrendt, A.,
553 Chepfer, H., Chiriaco, M., and Wulfmeyer, V.: Long-range transport of Saharan dust and its
554 radiative impact on precipitation forecast: a case study during the Convective and Orographically-
555 induced Precipitation Study (COPS), *Q. J. R. Meteorol. Soc.*, 137, 236–251, doi:10.1002/qj.719,
556 2011.

557 Chane Ming, F., Vignelles, D., Jegou, F., Berthet, G., Renard, J.-B., Gheusi, F., and Kuleshov, Y.:
558 Gravity-wave effects on tracer gases and stratospheric aerosol concentrations during the 2013
559 ChArMEx campaign, *Atmos. Chem. Phys.*, 16, 8023–8042, doi:10.5194/acp-16-8023-2016, 2016.

560 Chazette, P., Totems, J., Ancellet, G., Pelon, J., and Sicard, M.: Temporal consistency of lidar
561 observations during aerosol transport events in the framework of the ChArMEx/ADRI-MED
562 campaign at Minorca in June 2013, *Atmos. Chem. Phys.*, 16, 2863–2875, doi:10.5194/acp-16-2863-
563 2016, 2016.

564 Chester, R., Nimmo, M., and Keyse, S.: The influence of Saharan and Middle Eastern desert-derived
565 dust on the trace metal composition of Mediterranean aerosols and rainwater, in *The Impact of
566 Desert Dust Across the Mediterranean*, Guerzoni, S., and Chester, R., Eds., Kluwer, 253–273, 1996.



- 567 Choobari O. A., Zawar-Reza, P., and Sturman, A.: The global distribution of mineral dust and its
568 impacts on the climate system: A review, *Atmos. Res.*, 138, 152-165,
569 doi:10.1016/j.atmosres.2013.11.007, 2014.
- 570 D'Almeida, G. A. and Schütz, L.: Number, mass and volume distribution of mineral aerosol and soils of
571 the Sahara, *J. Climate Appl. Meteor.*, 22, 233-243, doi:10.1175/1520-
572 0450(1983)022<0233:NMAVDO>2.0.CO;2, 1983.
- 573 Denjean, C., Cassola, F., Mazzino, A., Triquet, S., Chevaillier, S., Grand, N., Bourriane, T., Momboisse,
574 G., Sellegri, K., Schwarzenbock, A., Freney, E., Mallet, M., and Formenti, P.: Size distribution and
575 optical properties of mineral dust aerosols transported in the western Mediterranean, *Atmos.*
576 *Chem. Phys.*, 16, 1081–1104, doi:10.5194/acp-16-1081-2016, 2016.
- 577 Doerenbecher, A., C. Basdevant, Ph. Drobinski, P. Durand, C. Fesquet, F. Bernard, Ph. Cocquerez, N.
578 Verdier and A. Vargas,: Low atmosphere drifting balloons: platforms for environment monitoring
579 and forecast improvement, *Bull. Amer. Meteor. Soc.*, 97, 1583–1599, doi:10.1175/BAMS-D-14-
580 00182.1.
- 581 Dubovik, O. and King, M. D.: A flexible inversion algorithm for retrieval of aerosol optical properties
582 from Sun and sky radiance measurements, *J. Geophys. Res.*, 105, 20673-20696,
583 doi:10.1029/2000JD900282, 2000.
- 584 Duce, R. A.: Sources, distributions, and fluxes of mineral aerosols and their relationship to climate, in
585 *Aerosol Forcing of Climate*, Charlson, R. J., and Heintzenberg, J., Eds., Wiley, 43-72, 1995.
- 586 Dulac, F. and Chazette, P.: Airborne study of a multi-layer aerosol structure in the eastern
587 Mediterranean observed with the airborne polarized lidar ALEX during a STAAARTE campaign (7
588 June 1997), *Atmos. Chem. Phys.*, 3, 1817-1831, doi:10.5194/acp-3-1817-2003, 2003.
- 589 Dulac, F., Buat-Ménard, P., Arnold, M., Ezat, U., and Martin, D: Atmospheric input of trace metals to
590 the western Mediterranean Sea: 1. Factors controlling the variability of atmospheric
591 concentrations, *J. Geophys. Res.*, 92, 8437-8453, doi:10.1029/JD092iD07p08437, 1987.
- 592 Dulac, F., Buat-Ménard, P., Ezat, U., Melki, S., and Bergametti, G. : Atmospheric input of trace metals
593 to the western Mediterranean: uncertainties in modelling dry deposition from cascade impactor
594 data, *Tellus*, 41B, 362-378, doi:10.1111/j.1600-0889.1989.tb00315.x, 1989.
- 595 Dulac, F., Bergametti, G., Losno, R., Remoudaki, E., Gomes, L., Ezat, U., and Buat-Ménard, P.: Dry
596 deposition of mineral aerosol particles: significance of the large size fraction, in *Precipitation*
597 *Scavenging and Atmosphere-Surface Exchange*, Schwartz, S. E., and Slinn W. G. N. Eds., 2, 841-
598 854, Hemisphere, Richland, WA, 1992a.
- 599 Dulac, F. Tanré, D., Bergametti, G., Buat-Ménard, P., Desbois, M., and Sutton, D. : Assessment of the
600 African airborne dust mass over the western Mediterranean Sea using Meteosat data, *J. Geophys.*
601 *Res.*, 97, 2489-2506, doi:10.1029/91JD02427, 1992b.
- 602 Ethé, C., Basdevant, C., Sadourny, R., Appu, K. S., Harenduprakash, L., Sarode, P. R., and Viswanathan,
603 G.: Air mass motion, temperature and humidity over the Arabian Sea and western Indian Ocean
604 during the INDOEX intensive phase, as obtained from a set of superpressure drifting balloons, *J.*
605 *Geophys. Res.*, 107, 8023, doi:10.1029/2001JD001120, 2002.
- 606 Ette, A. I. I.: The effect of the Harmattan dust on atmospheric electric parameters, *J. Atmos. Terr.*
607 *Phys.*, 33, 295-300, doi:10.1016/0021-9169(71)90208-X, 1971.
- 608 Farrell, W. M., Smith, P. H., Delory, G. T., Hillard, G. B., Marshall, J. R., Catling, D., Hecht, M., Tratt, D.
609 M., Renno, N., Desch, M. D., Cummer, S. A., Houser, J. G., and Johnson, B.: Electric and magnetic
610 signatures of dust devils from the 2000–2001 MATADOR desert tests, *J. Geophys. Res.*, 109,
611 E03004, doi:10.1029/2003JE002088, 2004.
- 612 Foret, G., Bergametti, G., Dulac, F. and Menuet, L.: An optimized particle size bin scheme for modeling
613 mineral dust aerosol, *J. Geophys. Res.*, 111, D17310, doi:10.1029/2005JD006797, 2006.
- 614 Formenti, P., Rajot, J. L., Desboeufs, K., Caquineau, S., Chevaillier, S., Nava, S., Gaudichet, A., Journet,
615 E., Triquet, S., Alfaro, S., Chiari, M., Haywood, J., Coe, H., and Highwood, E.: Regional variability of
616 the composition of mineral dust from western Africa: Results from the AMMA SOPO/DABEX and
617 DODO field campaigns, *J. Geophys. Res.*, 113, D00C13, doi:10.1029/2008JD009903, 2008.



- 618 Forsyth, B., Liu, B. Y. H., and Romay, F. J.: Particle charge distribution measurements for commonly
619 generated laboratory aerosol, *Aerosol Sci. Technol.*, 28, 489-501,
620 doi:10.1080/02786829808965540, 1998.
- 621 Francis, M., Renard, J.-B., Hadamcik, E., Couté, B., Gaubicher, B., and Jeannot, M.: New studies on
622 scattering properties of different kinds of soot, *J. Quant. Spectr. Rad. Transf.*, 112, 1766-1775,
623 doi:10.1016/j.jqsrt.2011.01.009, 2011.
- 624 Gheusi, F., Durand, P., Verdier, N., Dulac, F., Attié, J.-L., Commun, P., Barret, B., Basdevant, C., Clenet,
625 A., Derrien, S., Doerenbecher, A., El Amraoui, L., Fontaine, A., Hache, E., Jambert, C., Jaumouillé,
626 E., Meyerfeld, Y., Roblou, L., and Tocquer, F.: Adapted ECC ozonesonde for long-duration flights
627 aboard boundary-layer pressurised balloons, *Atmos. Meas. Tech.*, 9, 5811-5832, doi:10.5194/amt-
628 9-5811-2016, 2016.
- 629 Guerzoni, S., Chester, R., Dulac, F., Herut, B., Loÿe-Pilot, M.-D., Measures, C., Migon, C., Molinaroli, E.,
630 Moulin, C., Rossini, P., Saydam, C., Soudine, A., and Ziveri, P.: The role of atmospheric deposition
631 in the biogeochemistry of the Mediterranean Sea, *Prog. Oceanogr.*, 44, 147-190,
632 doi:10.1016/S0079-6611(99)00024-5, 1999.
- 633 Guieu, C., Ridame, C., Pulido-Villena, E., Bressac, M., Desboeufs, K., and Dulac, F.: Impact of dust
634 deposition on carbon budget: a tentative assessment from a mesocosm approach, *Biogeosci.*, 11,
635 5621-5635, doi:10.5194/bg-11-5621-2014, 2014.
- 636 Hamonou, E., Chazette, P., Balis, D., Dulac, F., Schneider, X., Galani, E., Ancellet, G., and Papayannis,
637 A.: Characterization of the vertical structure of Saharan dust export to the Mediterranean basin, *J.*
638 *Geophys. Res.*, 104, 22257-22270, doi:10.1029/1999JD900257, 1999.
- 639 Herut, B., Krom, M. D., Pan, G., and Mortimer, R.: Atmospheric input of nitrogen and phosphorus to
640 the Southeast Mediterranean: Sources, fluxes and possible impact, *Limnol. Oceanogr.*, 44, 1683-
641 1692, doi:10.4319/lo.1999.44.7.1683, 1999.
- 642 Jaenicke, R.: Aerosol physics and chemistry, in *Landolt-Börnstein Numerical Data and Functional*
643 *Relationships in Science and Technology V, 4b*, edited by Fischer, G., 391-457, Springer-Verlag,
644 Berlin, doi:10.1007/b31154, 1987.
- 645 Jeong, G. Y., Kim, J. Y., Seo, J., Kim, G. M., Jin, H. C., and Chun, Y.: Long-range transport of giant
646 particles in Asian dust identified by physical, mineralogical, and meteorological analysis, *Atmos.*
647 *Chem. Phys.*, 14, 505-521, doi:10.5194/acp-14-505-2014, 2014.
- 648 Johnston, A. M., Vincent, J. H., and Jones, A. D.: Electrical charge characteristics of dry aerosols
649 produced by a number of laboratory mechanical dispersers, *Aerosol Sci. Technol.*, 6, 115-127,
650 doi:10.1080/02786828708959125, 1987.
- 651 Li, X., Xingcai, L., and Xiaojing, Z.: Attenuation of an electromagnetic wave by charged dust particles
652 in a sandstorm, *Appl. Opt.*, 49, 6756-6761, doi:10.1364/AO.49.006756, 2010.
- 653 Li, Z., Lau, W. K.-M., Ramanathan, V., Wu, G., Ding, Y., Manoj, M. G., Liu, J., Qian, Y., Li, J., Zhou, T.,
654 Fan, J., Rosenfeld, D., Ming, Y., Wang, Y., Huang, J., Wang, B., Xu, X., Lee, S.-S., Cribb, M., Zhang, F.,
655 Yang, X., Zhao, C., Takemura, T., Wand, K., Xia, X., Yin, Y., Zhang, H., Guo, J., Zhai, P. M., Sugimoto,
656 N., Babu, S. S., and Brasseur, G. P.: Aerosol and monsoon climate interactions over Asia, *Rev.*
657 *Geophys.*, 54, 866-929, doi:10.1002/2015RG000500, 2016.
- 658 Linke, C., Möhler, O., Veres, A., Mohácsi, A., Bozóki, Z., Szabó, G., and Schnaiter, M.: Optical
659 properties and mineralogical composition of different Saharan mineral dust samples: a laboratory
660 study, *Atmos. Chem. Phys.*, 6, 3315-3323, doi:10.5194/acp-6-3315-2006, 2006.
- 661 Liu, J., Zheng, Y., Li, Z., Flynn, C., Welton, E. J., and Cribb, M.: Transport, vertical structure and
662 radiative properties of dust events in southeast China determined from ground and space
663 sensors, *Atmos. Environ.*, 45, 6469-6480, doi:10.1016/j.atmosenv.2011.04.031, 2011.
- 664 Loÿe-Pilot, M. D., Martin, J. M., and Morelli, J.: Influence of Saharan dust on the rain acidity and
665 atmospheric input to the Mediterranean, *Nature*, 321, 427-428, doi:10.1038/321427a0, 1986.
- 666 Lurton, T., Renard, J.-B., Vignelles, D., Jeannot, M., Akiki, R., Mineau, J.-L., and Tonnelier, T.: Light
667 scattering at small angles by atmospheric irregular particles: modelling and laboratory
668 measurements, *Atmos. Meas. Tech.*, 7, 931-939, doi:10.5194/amt-7-931-2014, 2014.



- 669 Maher, B. A., Prospero, J. M., Mackie, D., Gaiero, D., Hesse, P. P., and Balkanski, Y.: Global
670 connections between aeolian dust, climate and ocean biogeochemistry at the present day and at
671 the last glacial maximum, *Earth Sci. Rev.*, 99, 61–97, doi:10.1016/j.earscirev.2009.12.001, 2010.
- 672 Mahowald, N., S. Engelstaedter, S., Luo, C., Sealy, A., Artaxo, P., Benitez-Nelson, C., Bonnet, S., Chen,
673 Y., Chuang P. Y., Cohen, D. D., Dulac, F., Herut, B., Johansen, A. M., Kubilay, N., Losno, R.,
674 Maenhaut, W., Paytan, A., Prospero, J. M., Shank, L. M., and Siefert, R. L.: Atmospheric Iron
675 deposition: global distribution, variability and human perturbations, *Annu. Rev. Mar. Sci.*, 1, 245–
676 278, doi:10.1146/annurev.marine.010908.163727, 2009.
- 677 Mahowald, N., Ward, D. S., Kloster, S., Flanner, M. G., Heald, C. L., Heavens, N. G., Hess, P. G.,
678 Lamarque, J.-F., and Chuang P. Y.: Aerosol impacts on climate and biogeochemistry, *Annu. Rev.*
679 *Environ. Resour.*, 36, 45–74, doi:10.1146/annurev-environ-042009-0945072011, 2011.
- 680 Mallet, M., Dulac, F., Formenti, P., Nabat, P., Sciare, J., Roberts, G., Pelon, J., Ancellet, G., Tanré, D.,
681 Parol, F., Denjean, C., Brogniez, G., di Sarra, A., Alados-Arboledas, L., Arndt, J., Auriol, F., Blarel, L.,
682 Bourriane, T., Chazette, P., Chevaillier, S., Claeys, M., D'Anna, B., Derimian, Y., Desboeufs, K., Di
683 Iorio, T., Doussin, J.-F., Durand, P., Féron, A., Freney, E., Gaimoz, C., Goloub, P., Gómez-Amo, J. L.,
684 Granados-Muñoz, M. J., Grand, N., Hamonou, E., Jankowiak, I., Jeannot, M., Léon, J.-F., Maillé, M.,
685 Mailler, S., Meloni, D., Menut, L., Momboisse, G., Nicolas, J., Podvin, T., Pont, V., Rea, G., Renard,
686 J.-B., Roblou, L., Schepanski, K., Schwarzenboeck, A., Sellegri, K., Sicard, M., Solmon, F., Somot, S.,
687 Torres, B., Totems, J., Triquet, S., Verdier, N., Verwaerde, C., Waquet, F., Wenger, J., and Zapf, P.:
688 Overview of the Chemistry-Aerosol Mediterranean Experiment/Aerosol Direct Radiative Forcing
689 on the Mediterranean Climate (ChArMEx/ADRMED) summer 2013 campaign, *Atmos. Chem.*
690 *Phys.*, 16, 455–504, doi:10.5194/acp-16-455-2016, 2016.
- 691 Martin, J., Gordon, R. M., and Fitzwater, S. E.: The case for iron, *Limnol. Oceanogr.*, 36, 1793–1802,
692 doi:10.4319/lo.1991.36.8.1793, 1991.
- 693 Middleton, N. J., Betzer, P. R., and Bull, P. A.: Long-range transport of ‘giant’ aeolian quartz grains:
694 linkage with discrete sedimentary sources and implications for protective particle transfer, *Mar.*
695 *Geol.*, 177, 411–417, doi:10.1016/S0025-3227(01)00171-2, 2001.
- 696 Morales-Baquero, R., Pulido-Villena, E., and Reche, I.: Atmospheric inputs of phosphorus and
697 nitrogen to the southwest Mediterranean region: Biogeochemical responses of high mountain
698 lakes, *Limnol. Oceanogr.*, 51, 830–837, doi:10.4319/lo.2006.51.2.0830, 2006.
- 699 Moulin, C., Lambert, C. E., Dayan, U., Masson, V., Ramonet, M., Bousquet, P., Legrand, M., Balkanski,
700 Y. J., Guelle, W., Marticorena, B., Bergametti, G., and Dulac, F.: Satellite climatology of African
701 dust transport in the Mediterranean atmosphere, *J. Geophys. Res.*, 103, 13137–13144,
702 doi:10.1029/98JD00171, 1998.
- 703 Nabat, P., Solmon, F., Mallet, M., Kok, J. F. and Somot, S.: Dust emission size distribution impact on
704 aerosol budget and radiative forcing over the Mediterranean region: a regional climate model
705 approach, *Atmos. Chem. Phys.*, 12, 10545–10567, doi:10.5194/acp-12-10545-2012, 2012.
- 706 Nabat, P.; Somot, S.; Mallet, M.; Chiapello, I.; Morcrette, J. J., Solmon, F., Szopa, S., Dulac, F., Collins,
707 W., Ghan, S., Horowitz, L. W., Lamarque, J. F., Lee, Y. H., Naik, V., Nagashima, T., Shindell, D., and
708 Skeie, R.: A 4-D climatology (1979–2009) of the monthly tropospheric aerosol optical depth
709 distribution over the Mediterranean region from a comparative evaluation and blending of
710 remote sensing and model products, *Atmos. Meas. Tech.*, 6, 1287–1314, doi:10.5194/amt-6-1287-
711 2013, 2013.
- 712 Nabat, P., Somot, S., Mallet, M., Michou, M., Sevault, F., Driouech, F., Meloni, D., di Sarra, A., Di
713 Biagio, C., Formenti, P., Sicard, M., Léon, J.-F., and Bouin, M.-N.: Dust aerosol radiative effects
714 during summer 2012 simulated with a coupled regional aerosol–atmosphere–ocean model over
715 the Mediterranean, *Atmos. Chem. Phys.*, 15, 3303–3326, doi:10.5194/acp-15-3303-2015, 2015a.
- 716 Nabat, P., Somot, S., Mallet, M., Sevault, F., Chiacchio, M., and Wild, M.: Direct and semi-direct
717 aerosol radiative effect on the Mediterranean climate variability using a coupled regional climate
718 system model, *Clim. Dyn.*, 44, 1127–1155, doi:10.1007/s00382-014-2205-6, 2015b.
- 719 Nicoll, K. A., Harrison, R. G., and Ulanowski, Z.: Observations of Saharan dust layer electrification,
720 *Environ. Res. Lett.*, 6, 014001, doi:10.1088/1748-9326/6/1/014001, 2011.



- 721 Nihlén, T., Mattsson, J. O., Rapp, A., Gagaoudaki, C., Kornaros, G., and Papageorgiou, J.: Monitoring
722 of Saharan dust fallout on Crete and its contribution to soil formation. *Tellus B*, 47: 365–374.
723 doi:10.1034/j.1600-0889.47.issue3.7.x, 1995.
- 724 Omar, A. H., Winker, D. M., Kittaka, C., Vaughan, M. A., Liu, Z., Hu, Y., Trepte, C. R., Rogers, R. R.,
725 Ferrare, R. A., Lee, K.-P., Khuen, R. E., and Hostetler, C. A.: The CALIPSO automated aerosol
726 classification and lidar ratio selection algorithm, *J. Atmos. Oceanic Technol.*, 26, 1994–2014,
727 doi:10.1175/2009JTECHA1231.1, 2009.
- 728 Pey, J., Querol, X., Alastuey, A., Forastiere, F., and Stafoggia, M.: African dust outbreaks over the
729 Mediterranean Basin during 2001–2011: PM₁₀ concentrations, phenomenology and trends, and its
730 relation with synoptic and mesoscale meteorology, *Atmos. Chem. Phys.*, 13, 1395–1410,
731 doi:10.5194/acp-13-1395-2013, 2013.
- 732 Prodi, F. and Fea, G.: A case of transport and deposition of Saharan dust over the Italian Peninsula
733 and southern Europe, *J. Geophys. Res.*, 84, 6951–6960, doi:10.1029/JC084iC11p06951, 1979.
- 734 Prospero, J. M., Bonatti, E., Schubert, C., and Carlson, T. N.: Dust in the Caribbean atmosphere traced
735 to an African dust storm, *Earth Planet. Sci. Lett.*, 9, 287–293, doi:10.1016/0012-821X(70)90039-7,
736 1970.
- 737 Pye, K.: Aeolian dust transport and deposition over Crete and adjacent parts of the Mediterranean
738 Sea, *Earth Surf. Proc. Land.*, 17, 271–288. doi:10.1002/esp.3290170306, 1992.
- 739 Querol, X., Pey, J., Pandolfi, M., Alastuey, A., Cusack, M., Pérez, N., Moreno, T., Viana, M.,
740 Mihalopoulos, N., Kallos, G., and Kleanthous, S.: African dust contributions to mean ambient PM₁₀
741 mass-levels across the Mediterranean Basin, *Atmos. Environ.*, 43, 4266–4277,
742 doi:10.1016/j.atmosenv.2009.06.013, 2009.
- 743 Rea, G., Turquety, S., Menut, L., Briant, R., Mailler, S., and Siour, G.: Source contributions to 2012
744 summertime aerosols in the Euro-Mediterranean region, *Atmos. Chem. Phys.*, 15, 8013–8036,
745 doi:10.5194/acp-15-8013-2015, 2015.
- 746 Reche, I., Ortega-Retuerta, E., Romera O., Pulido Villena, E., Morales Baquero, R., and Casamayor, E.
747 O.: Effect of Saharan dust inputs on bacterial activity and community composition in
748 Mediterranean lakes and reservoirs, *Limnol. Oceanogr.*, 54, 869–879,
749 doi:10.4319/lo.2009.54.3.0869, 2009.
- 750 Reid, J. S., Kinney, J. E., Westphal, D. L., Holben, B. N., Welton, E. J., Tsay, S.-C., Eleuterio, D. P.,
751 Campbell, J. R., Christopher, S. A., Colarco, P. R., Jonsson, H. H., Livingston, J. M., Maring, H. B.,
752 Meier, M. L., Pilewski, P., Prospero, J. M., Reid, E. A., Remer, L. A., Russel, P. B., Savoie, D. L.,
753 Smirnov, A., and Tarré, D.: Analysis of measurements of Saharan dust by airborne and ground-
754 based remote sensing methods during the Puerto Rico Dust Experiment (PRIDE), *J. Geophys. Res.*,
755 108, 8586, doi:10.1029/2002JD002493, 2003a.
- 756 Reid, J. S., Jonsson, H. H., Maring, H. B., Smirnov, A., Savoie, D. L., Cliff, S. S., Reid, E. A., Livingston, J.
757 M., Meier, M. M., Dubovik, O., and Tsay, S.-C.: Comparison of size and morphological
758 measurements of coarse mode dust particles from Africa, *J. Geophys. Res.*, 108, 8593,
759 10.1029/2002JD002485, 2003b.
- 760 Reiff, J., Forbes, G. S., Spieksma, F. Th. M., and Reynders, J. J.: African dust reaching northwestern
761 Europe: A case study to verify trajectory Calculations, *J. Clim. Appl. Meteor.*, 25, 1543–1567,
762 doi:10.1175/1520-0450(1986)025<1543:ADRNEA>2.0.CO;2, 1986.
- 763 Renard, J.-B. Francis, M., Hadamcik, E., Daugeron, D., Couté, B., Gaubicher, B., and Jeannot, M.:
764 Scattering properties of sand. 2. Results for sands from different origins, *Appl. Opt.*, 49, 3552–
765 3559, doi:10.1364/AO.49.003552, 2010.
- 766 Renard, J.-B., Dulac, F., Berthet, G., Lurton, T., Vignelles, D., Jégou, F., Tonnelier, T., Jeannot, M.,
767 Couté, B., Akiki, R., Verdier, N., Mallet, M., Gensdarmes, F., Charpentier, P., Mesmin, S., Duverger,
768 V., Dupont, J.-C., Elias, T., Crenn, V., Sciare, J., Zieger, P., Salter, M., Roberts, T., Giacomoni, J.,
769 Gobbi, M., Hamonou, E., Olafsson, H., Dagsson-Waldhauserova, P., Camy-Peyret, C., Mazel, C.,
770 Décamps, T., Piringer, M., Surcin, J., and Daugeron, D.: LOAC, a light aerosols counter for ground-
771 based and balloon measurements of the size distribution and of the main nature of atmospheric



- 772 particles, 1. Principle of measurements and instrument evaluation, *Atmos. Meas. Tech.*, 9, 1721-
773 1742, doi:10.5194/amt-9-1721-2016, 2016a.
- 774 Renard, J.-B., Dulac, F., Berthet, G., Lurton, T., Vignelles, D., Jégou, F., Tonnelier, T., Jeannot, M.,
775 Couté, B., Akiki, R., Verdier, N., Mallet, M., Gensdarmes, F., Charpentier, P., Mesmin, S., Duverger,
776 V., Dupont, J.-C., Elias, T., Crenn, V., Sciare, J., Zieger, P., Salter, M., Roberts, T., Giacomoni, J.,
777 Gobbi, M., Hamonou, E., Olafsson, H., Dagsson-Waldhauserova, P., Camy-Peyret, C., Mazel, C.,
778 Décamps, T., Piringier, M., Surcin, J., and Daugeron, D.: LOAC, a light aerosols counter for ground-
779 based and balloon measurements of the size distribution and of the main nature of atmospheric
780 particles, 2. First results from balloon and unmanned aerial vehicle flights, *Atmos. Meas. Tech.*, 9,
781 3673-3686, doi:10.5194/amt-9-3673-2016, 2016b.
- 782 Schmid, B., Livingston, J. M., Russell, P. B., Durkee, P. A., Jonsson, H. H., Collins, D. R., Flagan, R. C.,
783 Seinfeld, J. H., Gassó, S., Hegg, D. A., Öström, E., Noone, K. J., Welton, E. J., Voss, K. J., Gordon, H.
784 R., Formenti, P., and Andreae, M. O.: Clear-sky closure studies of lower tropospheric aerosol and
785 water vapor during ACE-2 using airborne sunphotometer, airborne in-situ, space-borne, and
786 ground-based measurements., *Tellus B*, 52, 568–593. doi:10.1034/j.1600-0889.2000.00009.x,
787 2000.
- 788 Schütz, L., Jaenicke, R., and Pietrek, H.: Saharan dust transport over the North Atlantic Ocean, *Geol.*
789 *Soc. Am. Spec. Pap.*, 186, 87-100, doi:10.1130/SPE186-p87, 1981.
- 790 Slinn, W. G. N.: Air to sea transfer of particles, in *Air-sea exchange of gases and particles*, Liss, P. S.,
791 and Slinn, W. G. N. Eds., N.A.T.O. AS1 Series, Reidel, Dordrecht, Holland, 299-396, 1983.
- 792 Sow, M., Crase, E., Rajot, J. L., Sankaran, R. M., and Lacks, D. J.: Electrification of particles in dust
793 storms : Field measurements during the monsoon period in Niger, *Atmos. Res.*, 102, 343-350,
794 doi:10.1016/j.atmosres.2011.08.010, 2011.
- 795 Swap, R., Garstang, M., Greco, S., Talbot, R. and Kållberg, P.: Saharan dust in the Amazon Basin, *Tellus*
796 *B*, 44, 133–149, doi:10.1034/j.1600-0889.1992.t01-1-00005.x, 1992.
- 797 Stokes, G. G.: On the effect of the internal friction of fluids on the motion of pendulums, *Trans.*
798 *Cambridge Philos. Soc.*, 9, 51-52, 1851.
- 799 Thieuleux, F., Moulin, C., Bréon, F.M., Maignan, F., Poitou, J., and Tanré, D.: Remote sensing of
800 aerosols over the oceans using MSG/SEVIRI imagery, *Ann. Geophys.*, 23, 3561-3568,
801 doi:10.5194/angeo-23-3561-2005, 2005.
- 802 Ulanowski, Z., Bailey, J., Lucas, P.W., Hough, J.H., and Hirst, E.: Alignment of atmospheric mineral
803 dust due to electric field, *Atmos. Chem. Phys.*, 7, 6161-6173, doi:10.5194/acp-7-6161-2007, 2007.
- 804 Vincent, J., Laurent, B., Losno, R., Bon Nguyen, E., Roullet, P., Sauvage, S., Chevaillier, S., Coddeville,
805 P., Ouboulmane, N., di Sarra, A. G., Tovar-Sánchez, A., Sferlazzo, D., Massanet, A., Triquet, S.,
806 Morales Baquero, R., Fornier, M., Coursier, C., Desboeufs, K., Dulac, F., and Bergametti, G.:
807 Variability of mineral dust deposition in the western Mediterranean basin and south-east of
808 France, *Atmos. Chem. Phys.*, 16, 8749-8766, doi:10.5194/acp-16-8749-2016, 2016.
- 809 Weinzierl, B., Petzold, A., Esselborn, M., Wirth, M., Rasp, K., Kandler, K., Schütz, L., Koepke, P., and
810 Fiebig, M.: Airborne measurements of dust layer properties, particle size distribution and mixing
811 state of Saharan dust during SAMUM 2006, *Tellus B*, 61, 96–117, 2009.
- 812 Weiss-Wrana, K.: Optical properties of interplanetary dust - Comparison with light scattering by
813 larger meteoritic and terrestrial grains, *Astron. Astrophys.*, 126, 240-250, 1983.
- 814 Winker, D. M., Vaughan, M. A., Omar, A., Hu, Y., Powell, K. A., Liu, Z., Hunt, W. H., and Young, S. A.:
815 Overview of the CALIPSO mission and CALIOP data processing algorithms, *J. Atmos. Oceanic*
816 *Technol.*, 26, 2310-2323, doi:10.1175/2009JTECHA1281.1, 2009.
- 817 Zannoni, N., Gros, V., Sarda Esteve, R., Kalogridis, C., Michoud, V., Dusanter, S., Sauvage, S., Locoge,
818 N., Colomb, A., and Bonsang, B.: Summertime OH reactivity from a receptor coastal site in the
819 Mediterranean basin, *Atmos. Chem. Phys. Discuss.*, doi:10.5194/acp-2016-684, submitted, 2017.
- 820 Zender, C. S., H. Bian, and D. Newman, Mineral Dust Entrainment and Deposition (DEAD) model:
821 Description and 1990s dust climatology, *J. Geophys. Res.*, 108(D14), 4416,
822 doi:10.1029/2002JD002775, 2003.



823

824

825

826

827

828

829

830

831

832

833

834

835

836

837

838

839

840

841

842

843

844

845

846

847

848

849

850

851

852

853

854

855

Date (2013)	Time (UT)		Altitude range (km)	Launch site
	start	end		
15 June	22:12	22:48	0.9 – 6.9	
16 June	10:37	11:14	2.0 – 12.1	
16 June	21:17	21:59	0.2 – 10.1	
17 June	10:02	10:41	0.1 – 11.4	
17 June	18:29	20:33	0.9 – 33.3	
18 June	16:35	18:41	0.2 – 35.4	Cap d'en Font, Minorca Isl., Spain (39.88°N, 4.25°E)
18 June	21:19	22:39	0.4 – 21.5	
19 June	10:15	12:03	0.8 – 30.7	
19 June	13:50	15:03	0.3 – 20.7	
28 June	05:38	07:54	0.6 – 36.0	
29-30 June	23:31	01:49	0.2 – 35.9	
30 June	14:03	15:46	0.1 – 26.8	
2 July	10:30	12:24	0.7 – 32.8	
27-28 July	23:13	01:17	0.3 – 33.5	Levant Isl., France (43.02°N, 6.46°E)
28 July	15:31	18:06	0.3 – 33.3	
3 August	11:04	12:35	0.3 – 21.7	
4 August	15:32	17:36	0.2 – 32.2	

Table 1. List of the seventeen LOAC flights under Light Dilatable Balloons (LDB) flown during African dust plume events of the ChArMEx summer 2013 campaign.



856

Balloon #	Date (2013)	Time slot of LOAC data (UT)		Drift altitude (km)	Latitude, longitude at end of flight	Flight length (km)	Ceiling duration (h)
		start	end				
B74	16 June	10:00	21:28	2.1	42.892°N, 05.229°E	361	11.3
B70	16 June	09:51	23:01	3.1	40.182°N, 06.128°E	164	12.6
B75	17 June	09:31	16:23	2.0	42.815°N, 03.811°E	362	6.4
B72	17 June	17:11	18:59	2.75	43.179°N, 04.800°E	377	7.0
B77	19 June	10:25	16:54	2.55	43.042°N, 04.833°E	369	6.0
B71	19 June	10:29	15:58	3.3	43.041°N, 05.151°E	363	3.6
B80	27-28 June	09:50	12:31	3.0	37.916°N, 12.145°E	719	25.3
B73	28 June	05:25	16:42	2.7	37.523°N, 08.830°E	512	11.2
B76	2-3 July	13:04	09:14	3.2	37.880°N, 12.109°E	717	19.3
B82	3 August	06:12	08:12	3.0	43.077°N, 06.662°E	45	1.4

857

858 **Table 2.** List of the ten LOAC flights aboard drifting Boundary Layer Pressurized Balloons (BLPBs)
 859 flown during African dust plume events of the ChArMEx summer 2013 campaign. All balloons were
 860 launched from Minorca Isl. (Spain; 39.864°N, 4.255°N) except B82 that was launched from the Levant
 861 Isl. (France; 43.022°N, 6.460°E).



862

Date (2013)	Altitude (km)	Average volume median diameter (D_m , μm) \pm standard deviation (number of measurements)		
		Mode 1	Mode 2	Mode 3
16 June	2.1	0.22 \pm 0.02 (32)	3.6 \pm 0.8 (32)	30.6 \pm 3.4 (32)
	3.1	0.30 \pm 0.07 (31)	3.3 \pm 0.3 (31)	28.5 \pm 1.7 (30)
17 June	2.0	0.26 \pm 0.02 (17)	4.1 \pm 0.6 (17)	27.4 \pm 4.1 (17)
	2.8	0.24 \pm 0.02 (16)	3.3 \pm 0.5 (16)	30.9 \pm 5.9 (16)
19 June	2.6	0.25 \pm 0.01 (28)	3.5 \pm 0.6 (28)	32.8 \pm 4.7 (27)
	3.3	0.26 \pm 0.01 (48)	4.5 \pm 0.5 (48)	32.4 \pm 4.2 (41)
<i>Average</i>		<i>0.26 \pm 0.04</i>	<i>3.7 \pm 0.4</i>	<i>30.4 \pm 2.8</i>

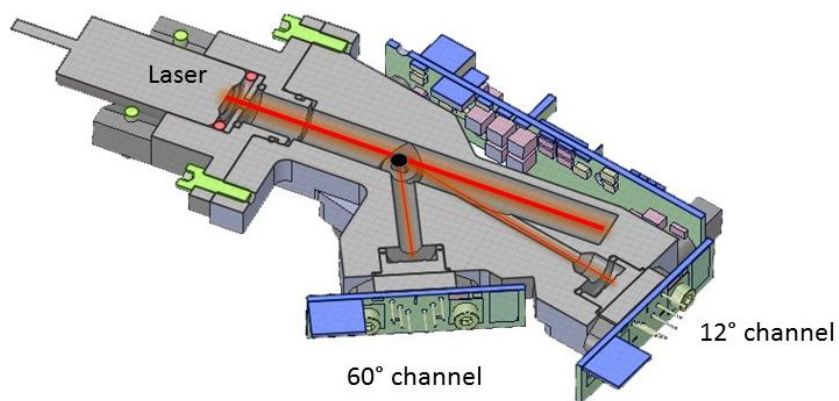
863

864 **Table 3.** Average volume median diameter (D_m) of the three fitted aerosol particle modes and
865 respective standard deviation along BPCL flights at float altitude within dust layers, for the 6 BPCLs
866 launched from Minorca during the 16-19 June 2013 dust event. The time evolution for the three pairs
867 of BPCL flights flown during this period is shown in Figure 15. The average and standard deviation in
868 the bottom line are obtained by averaging the 6 above values.

869



870 |
871

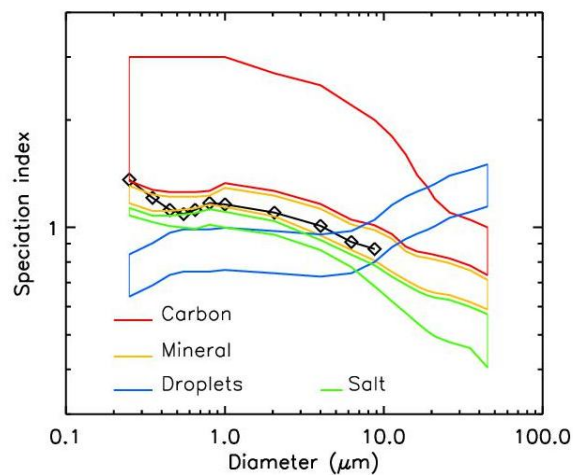


872
873
874
875

Figure 1. The LOAC instrument and principle of scattering measurements at two angles.



876



877

878

879

880

881

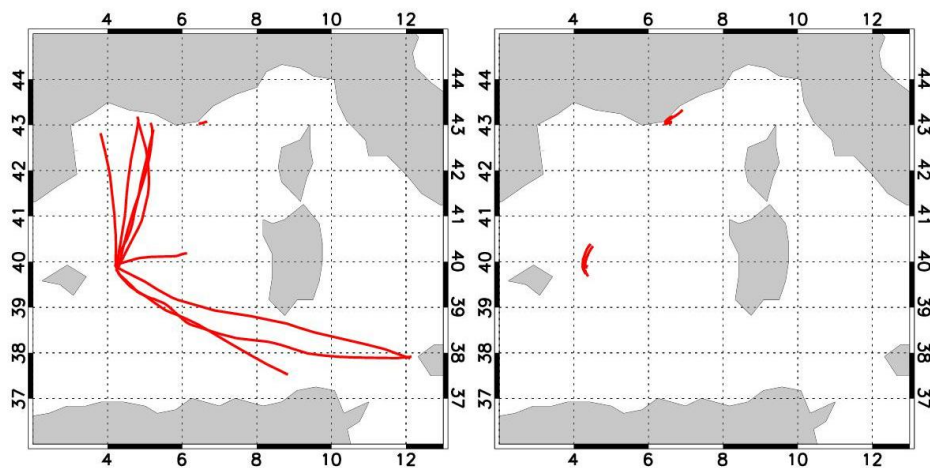
882

883

Figure 2. “Speciation zones” obtained in laboratory for several types of particles (color lines) and an example of LOAC speciation index obtained during ambient air measurements inside a Saharan dust plume at an altitude of 3.1 km (18 June 2013, 18:15 UT) above Minorca, Spain (diamonds).



884

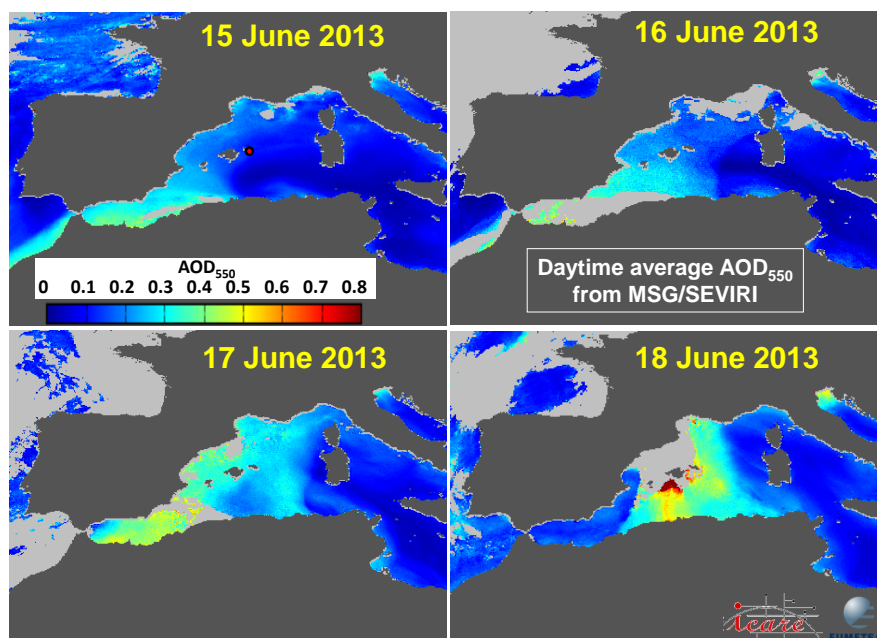


885
886
887
888
889

Figure 3. Trajectories of the flights for the 10 BLPBs (left) and 17 LDBs (right).



890



891

892

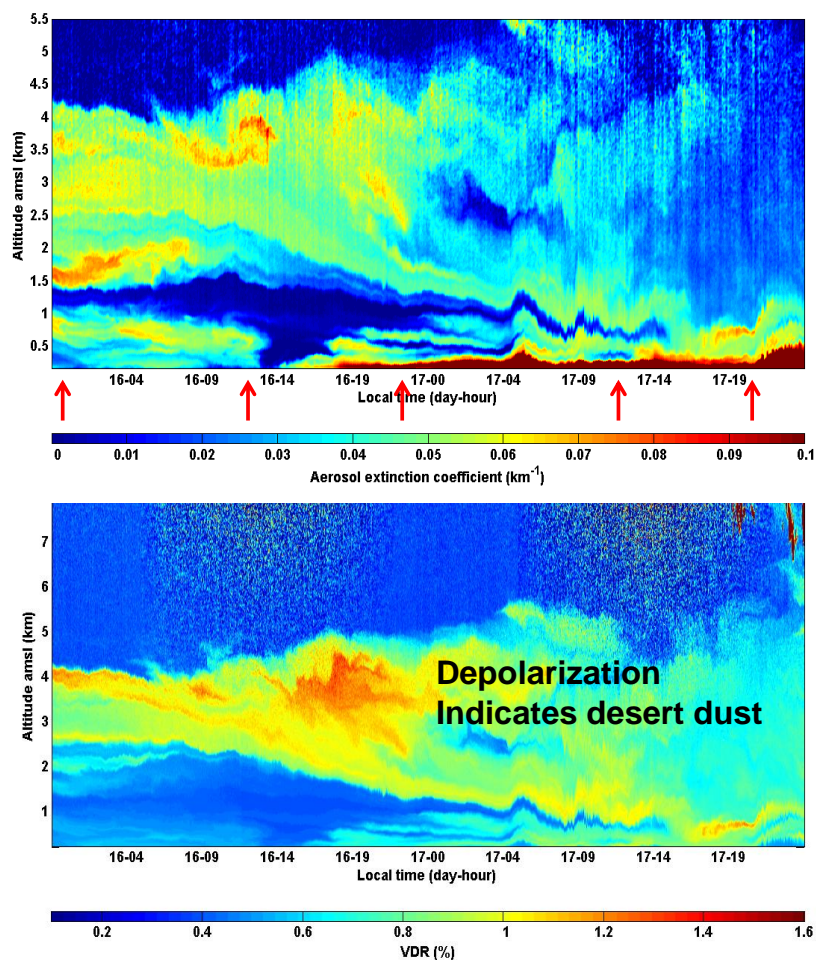
893 **Figure 4.** Daytime averaged Meteosat-derived AOD at 550 nm over seawater from June 15 to 18,
894 2013, showing the synoptic development of the dust event. The product is computed by the ICARE
895 data and services center (<http://www.icare.univ-lille1.fr>) based on the algorithm of Thieuleux et al.
896 (2005). Lands are masked in dark grey and clouds over ocean in light grey. The red dot on the 15 June
897 image indicates the balloon launching site and remote sensing station on Minorca Island.

898

899



900



901

902

903 **Figure 5.** Lidar-derived time-height cross-sections of the aerosol extinction (top) and volume

904 depolarization ratio (bottom) at Minorca from June 15, 22:00 to 17, 24:00 UT. The red arrows

905 indicate the time of the 5 LDB launches. Courtesy of P. Chazette and J. Totems, after Chazette et al.

906 (2016).

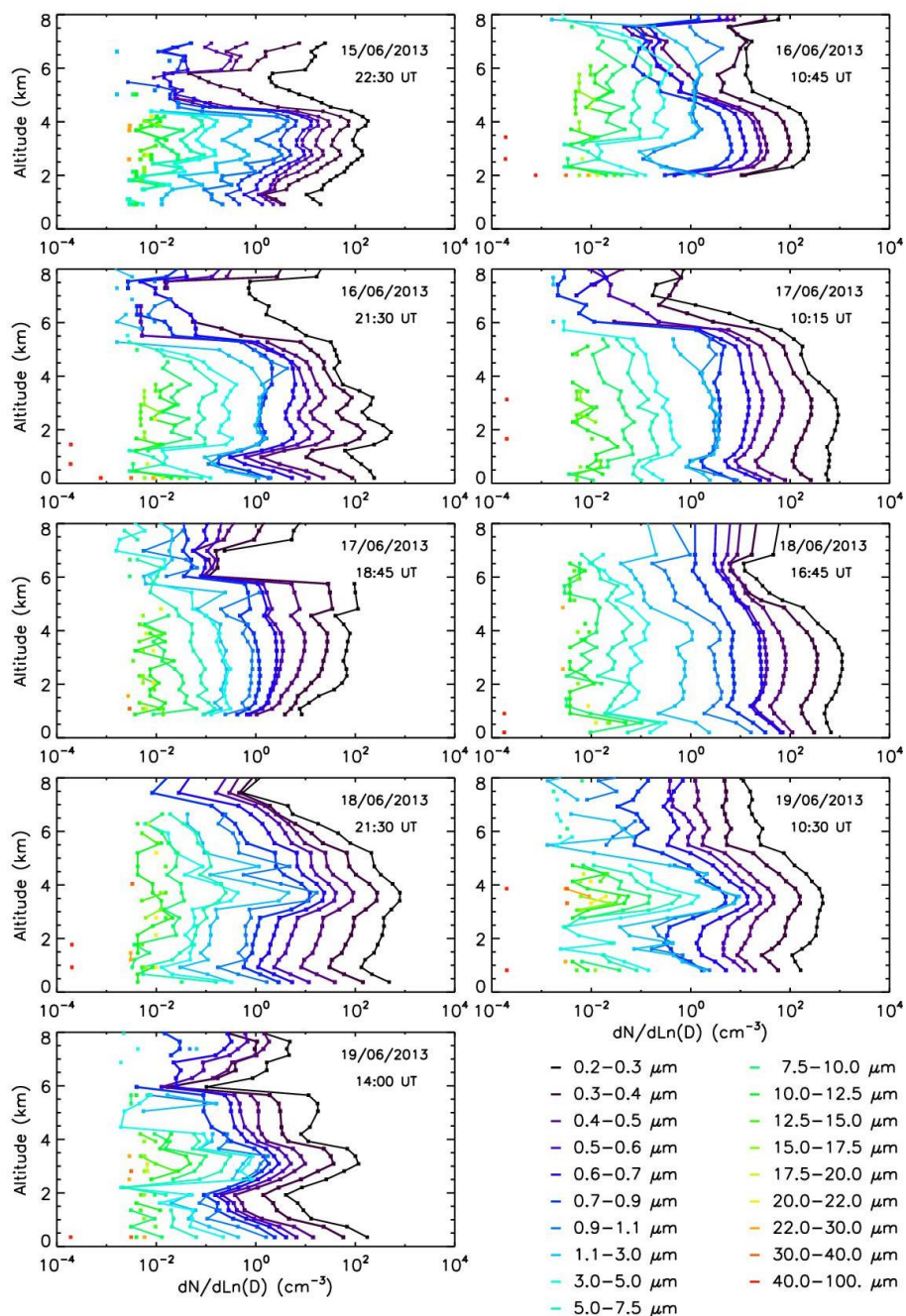
907

908

909



910

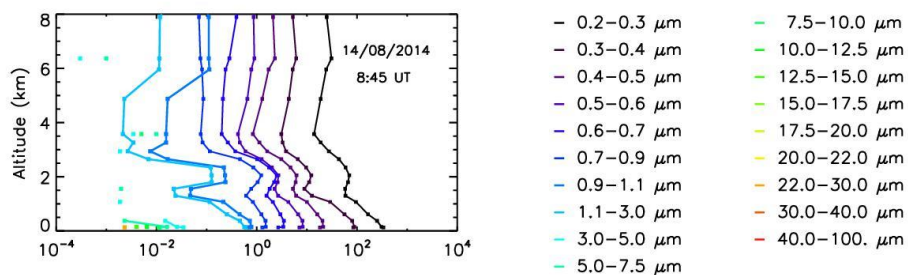


911
 912

913 **Figure 6.** Evolution of the dust plume from LOAC balloon measurements over Minorca, Spain, from
 914 15 to 19 June. The ascent from 0 to 8 km takes about 30 min and the reported times of measurement
 915 are taken at the middle of the profile.



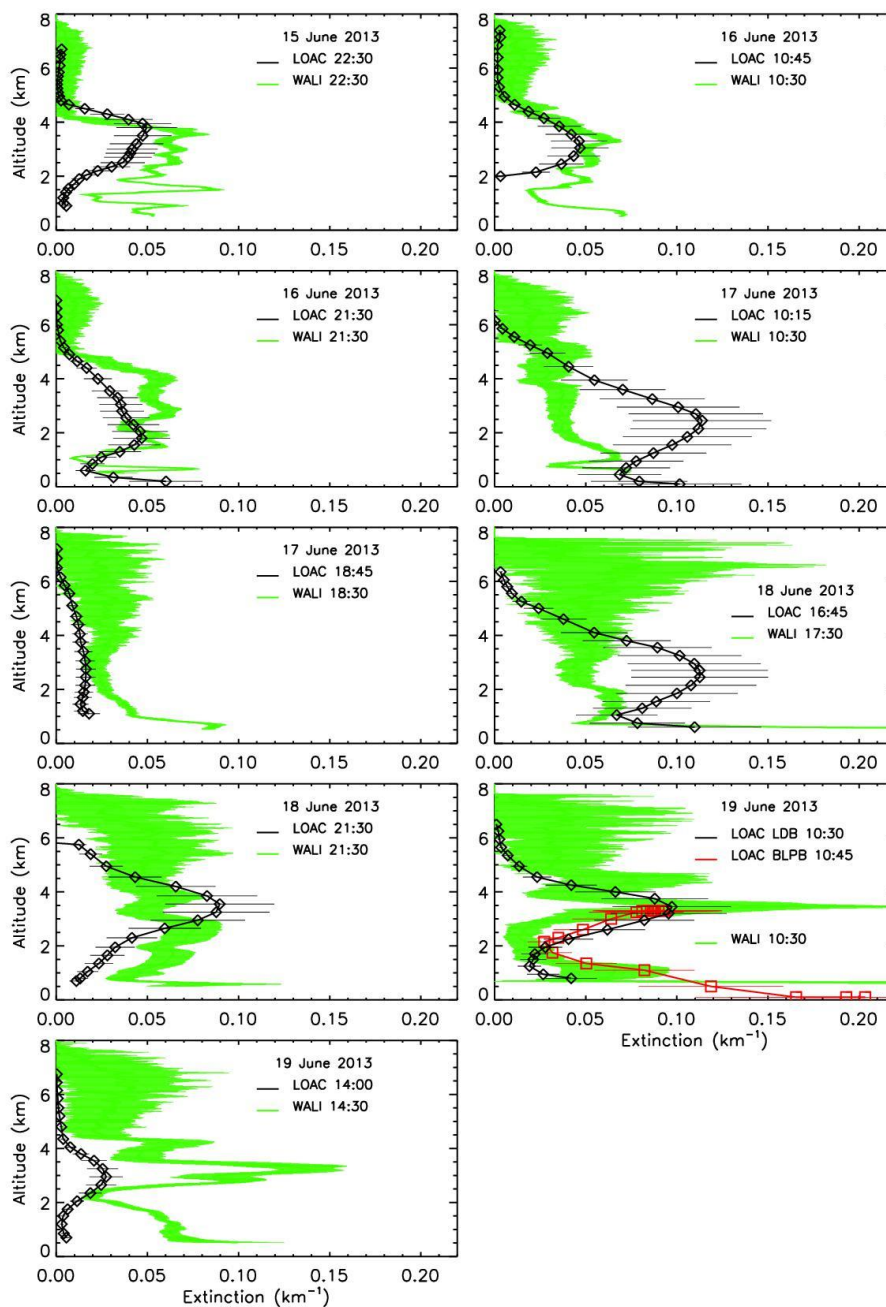
916



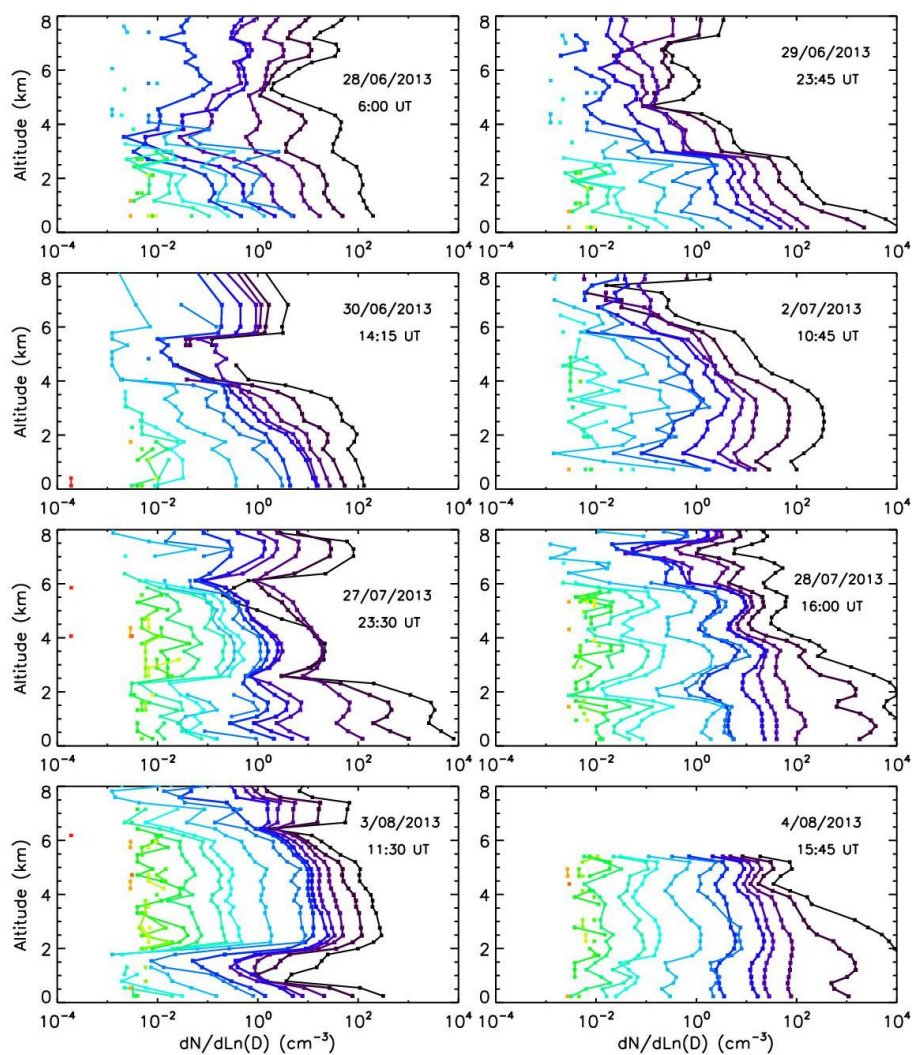
917

918 **Figure 7.** Typical vertical profile when no dust is present; flight from Aire sur l'Adour (South West of
919 France), on 14 August 2014.

920



921
922 **Figure 8.** Comparison between LOAC extinctions and WALI lidar extinction at 350 nm. The LOAC error
923 bars consider the uncertainty on the LOAC measurements and on the counting-extinction conversion;
924 the WALI error bars are calculated from the individual measurement scatter.
925

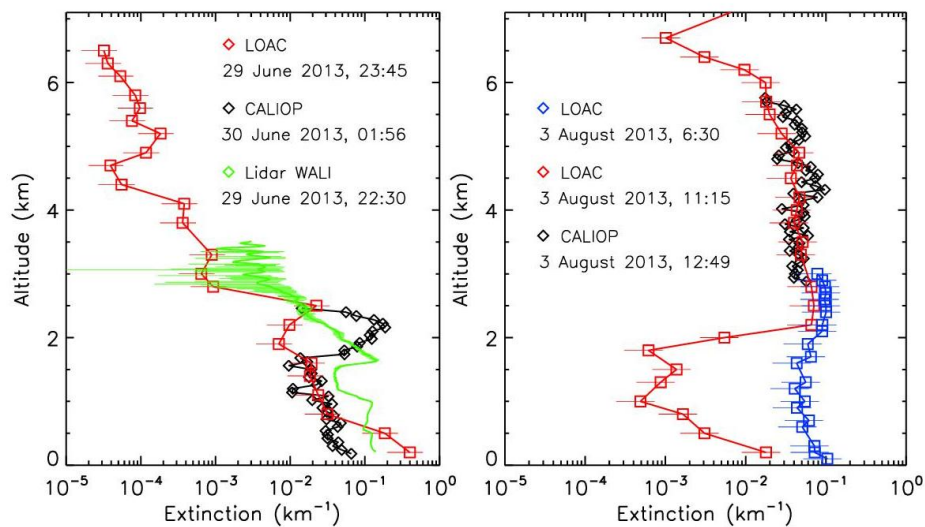


926
927

928 **Figure 9.** Same as Fig. 6 but for other sand plume events observed over Minorca (27 June – 2 July)
929 and Ile du Levant (27 July - 4 August).



930



931

932

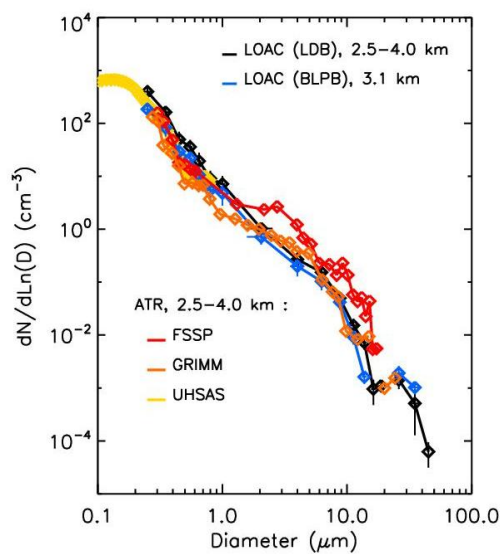
933 **Figure 10.** Left, vertical profiles of aerosol extinction from LOAC, CALIOP and WALI for the 29-30 June
 934 event, above Minorca; right, vertical profiles of aerosol extinction from LOAC (LDB and BLPB flights)
 935 and CALIOP for the 3 August event above Ile du Levant.

936

937



938



939

940

941 **Figure 11.** Comparison of the particle size distributions during the 16 June dust plume event over

942 Minorca, obtained with LOAC instruments under balloons and particle counters on board the ATR-42

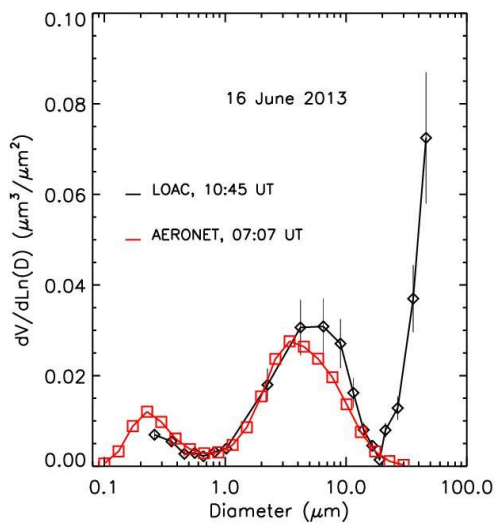
943 aircraft; measurement altitudes are given.

944

945



946



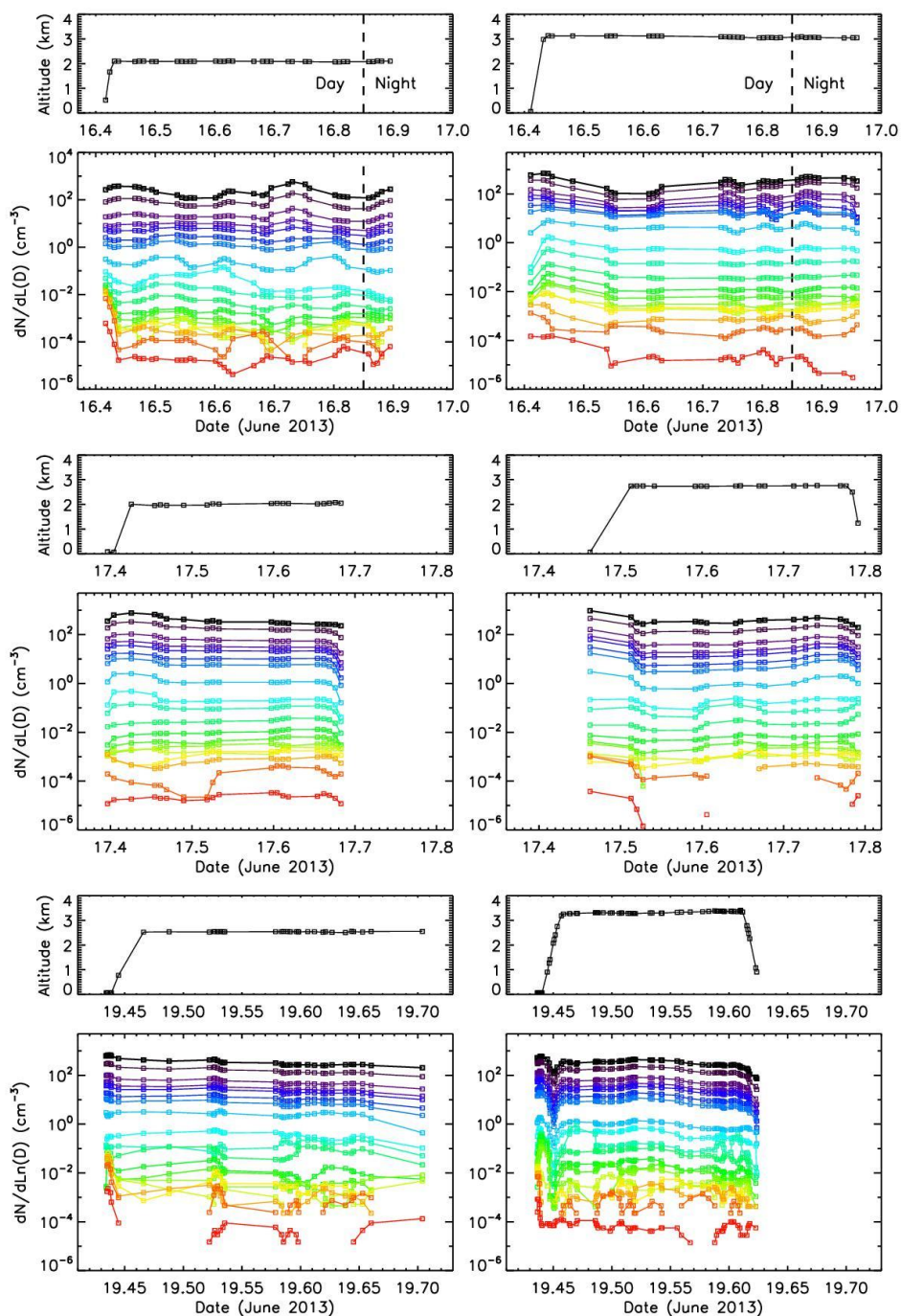
947

948

949 **Figure 12.** Volume size distribution retrieved from AERONET (<https://aeronet.gsfc.nasa.gov/>) and

950 LOAC data on 16 June at Minorca.

951

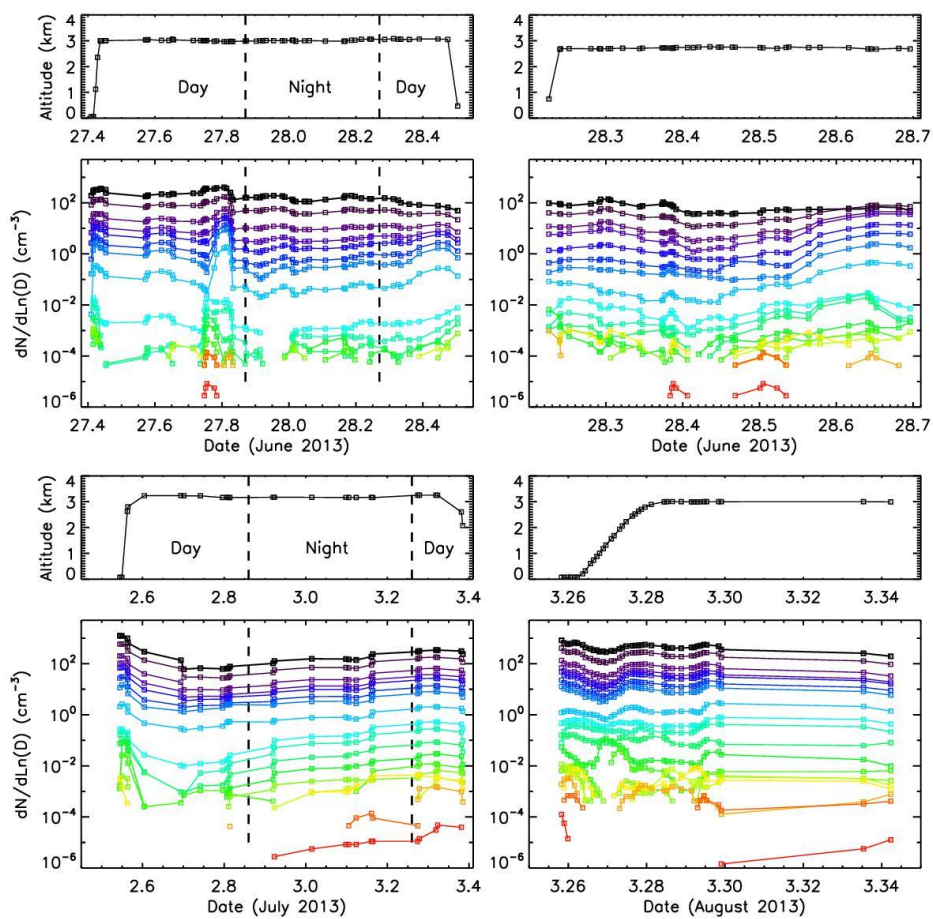


952
953

954 **Figure 13.** Flight altitude (up) and time evolution (bottom) of the LOAC-derived aerosol concentration
955 for the 19 size classes, from BLPB flights from Minorca towards French coast. Colour coding is as in
956 Fig. 6. Day-night transitions are indicated when appropriate.



957



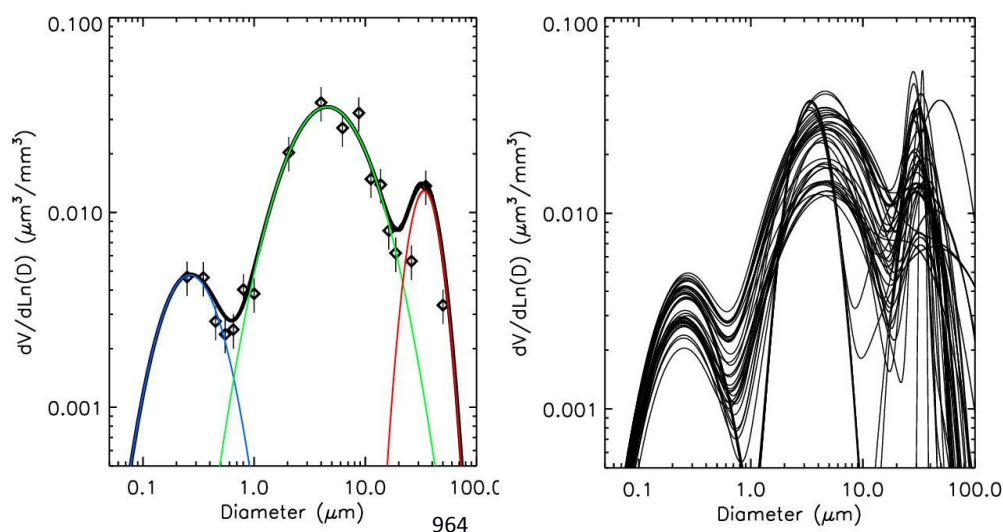
958

959

960

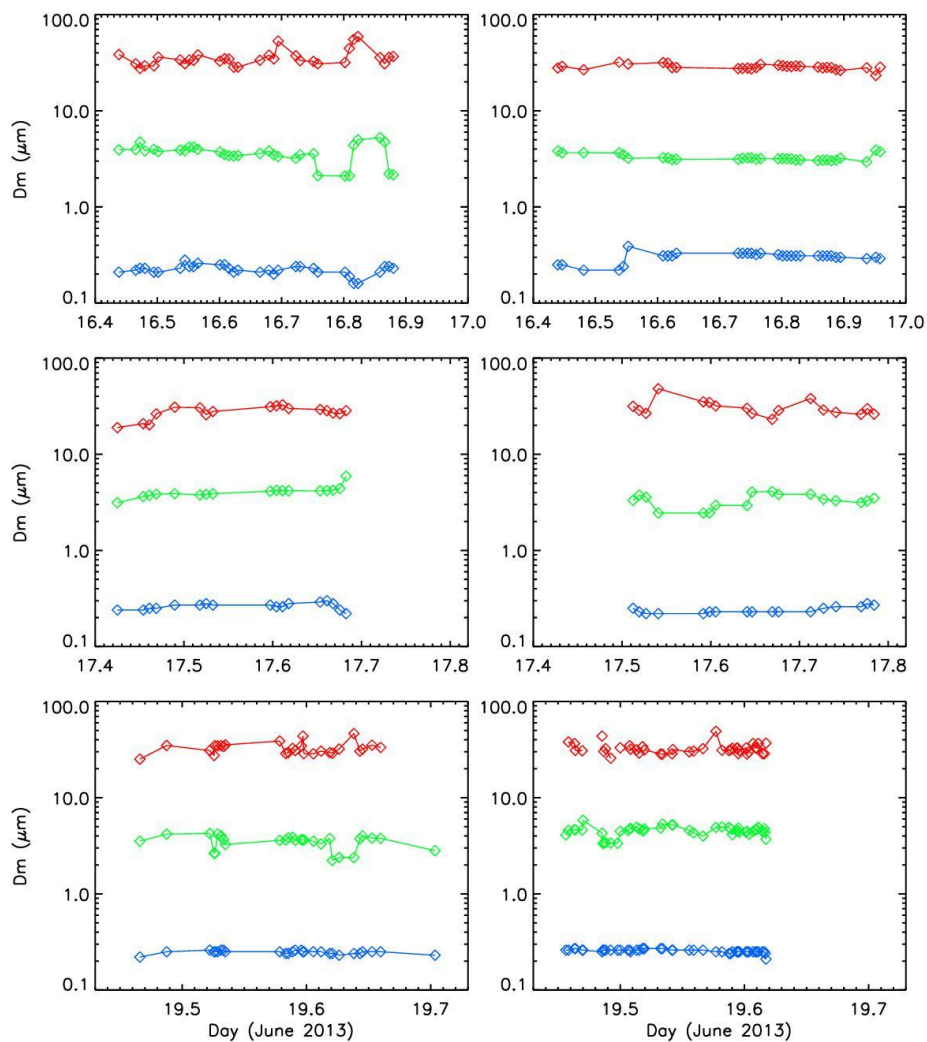
961

Figure 13, continued.



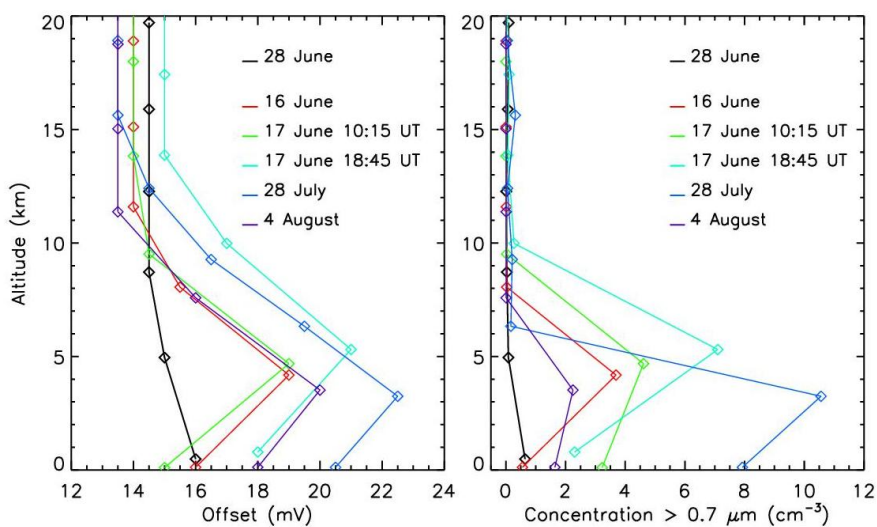
962
963
965
966
967
968
969
970
971
972

Figure 14. Left: Particle volume size distribution within the desert dust plume from the BLPB of 19 June at an altitude of 3.3 km (12:30 UT). The black diamonds are the LOAC measurements, the coloured curves represent the lognormal functions for each of the observed modes, and the black curve represents the overall fit (sum of the 3 modes). The geometric mean diameters (D_m) of the 3 modes are of 0.27, 4.6 and 34 μm , respectively, with respective geometric standard deviations (σ) of 1.79, 2.14 and 1.35. Right: The 41 fitted size distributions when the third mode was detected, retrieved from measurements at BLPB float altitude.



973
974
975
976
977
978
979
980
981

Figure 15. Time-evolution of the particle size at the maximum concentration for each mode (D_m) of the volume size distribution, at float altitude of BLPB flights from Minorca towards French coast. The altitudes are 2.1 and 3.1 km for the 16 June flights (top left and right, respectively), 2.0 and 2.7 km for the 17 June flights (middle left and right, resp.), and 2.5 and 3.3 km for the 19 June flights (bottom left and right, resp.). Average D_m values of the 3 modes during each flight are given in Table 3.



982

983

984

985

986

987

988

Figure 16. Left: Profiles of the LOAC electronic offset in case of crossing a strong dust plume (16 June, 17 June mid-time and evening, 28 July and 4 August) and in case of a weak dust plume just close to ground on 28 June. Right: Profiles of number concentrations of dust particles larger than 0.7 μm for the same flights.